12 Hadron structure and the parton model

Introduction · Elastic electron–muon scattering · Elastic electron–proton scattering · Inelastic electron–proton scattering · Bjorken scaling and the parton model · Quark structure of the nucleon · The Drell–Yan process · Quark jets in e^+e^- annihilation

12.1 Introduction

The modern approach to the study of hadron structure has its origins in the pioneering work of Hofstadter and collaborators at Stanford who, in the 1950s, used beams of electrons to probe the electric charge distributions of nuclei. This work was described in section 3.3. Here, we reiterate the principles of the technique in order to establish a theoretical framework in which the results of more recent experiments may be explained.

Consider Coulomb scattering of an electron by a stationary point proton as shown in figure 12.1. The scattering process is viewed as the emission by the proton of a virtual photon which, when absorbed by the initial electron with momentum $\boldsymbol{p}_i$, produces the final state electron with momentum $\boldsymbol{p}_f$. The differential cross-section for this process is the well-known Rutherford formula given in equation (1.15) but modified for a relativistic particle by writing $\mu v_1^2 = p_i c$. In natural units (appendix F) the formula then becomes

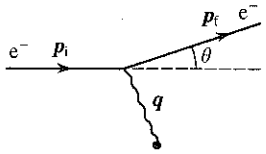

Figure 12.1
Coulomb scattering of an electron by a stationary point proton.

$$\frac{d\sigma}{d\Omega} = \frac{\alpha^2}{4p_i^2 \sin^4(\theta/2)}. \tag{12.1}$$

The change in momentum of the electron, or momentum transfer, is equal

to the momentum $\boldsymbol{q}$ of the virtual photon:

$$\boldsymbol{q} = \boldsymbol{p}_i - \boldsymbol{p}_f \qquad \text{or} \qquad q^2 = p_i^2 + p_f^2 - 2\boldsymbol{p}_i \cdot \boldsymbol{p}_f.$$

For a stationary proton $|\boldsymbol{p}_i| = |\boldsymbol{p}_f|$ and

$$q^2 = 2p_i^2(1 - \cos\theta) = 4p_i^2 \sin^2(\theta/2).$$

Furthermore, since

$$d\Omega = 2\pi d(\cos\theta) = \pi dq^2/p_i^2$$

the Rutherford scattering formula may be written as

$$\frac{d\sigma}{dq^2} = \frac{4\pi\alpha^2}{q^4}. \tag{12.2}$$

In reality, the charge of the proton is not localized at a point. In order to determine the charge distribution the measured differential cross-section for scattered electrons could in principle be compared with that expected for scattering from a point charge (the Rutherford cross-section) and expressed in the form

$$\left(\frac{d\sigma}{d\Omega}\right)_{\text{measured}} = \left(\frac{d\sigma}{d\Omega}\right)_{\text{Rutherford}} [F(\boldsymbol{q})] \tag{12.3}$$

where $F(\boldsymbol{q})$, the *form factor*,* is the Fourier transform of the electric charge density distribution:

$$F(\boldsymbol{q}) = \int \rho(\boldsymbol{r}) \exp(i\boldsymbol{q}\cdot\boldsymbol{r})\, d\tau. \tag{12.4}$$

However, even if the proton is considered as point-like the Rutherford calculation can readily be improved by treating the electron as a spin $\frac{1}{2}$ Dirac particle and allowing the proton to recoil. This situation is depicted in figure 12.2 and the relativistic treatment leads to the Mott[1] formula which may be expressed as

$$\left(\frac{d\sigma}{d\Omega}\right)_{\text{Mott}} = \left(\frac{d\sigma}{d\Omega}\right)_{\text{Rutherford}} \frac{\cos^2(\theta/2)}{1 + (2E/M)\sin^2(\theta/2)} \tag{12.5}$$

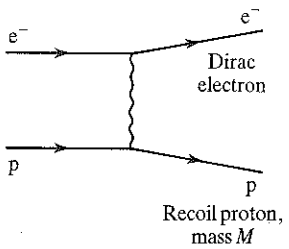

Figure 12.2
Feynman diagram for the Coulomb scattering of an electron by a proton.

* The form factor may be expressed in the form shown in equation (3.12) by integrating over the angle variable and dividing by the nuclear charge Ze. See also examples 12.3 and 12.4.

where E is the energy of the incident electron and M is the proton mass. Still further improvements can be made to the Mott formula if the proton is treated as a spin $\frac{1}{2}$ Dirac-type particle. The electron will be influenced not only by the electric charge of the proton but also by its magnetic moment which is known to be anomalous with a value of 2.79 nuclear magnetons. This gives rise to two form factors, electric and magnetic. A calculation based on these further considerations was performed by Rosenbluth,[2] and it is more appropriate to compare measured differential cross-sections with the Rosenbluth formula rather than the Rutherford or Mott formulae. In its essentials the Rosenbluth formula is

$$\frac{d\sigma}{d\Omega} = \left(\frac{d\sigma}{d\Omega}\right)_{\text{Mott}} [A(q^2) + B(q^2) \tan^2(\theta/2)] \tag{12.6}$$

where the two form factors A and B are now functions of the square of the four-momentum transfer.

Figure 12.3 shows the differential cross-section for the elastic scattering of 188 MeV electrons from hydrogen measured by Hofstadter and McAllister.[3] The figure shows that at large scattering angles the measured differential cross-section is less than predicted by the Rosenbluth formula indicating that the proton has a diffuse structure.

With the advent of the two-mile linear accelerator at SLAC higher energy electron beams became available leading to much higher q^2 (shorter wavelength) probes which gave access to the so-called deep

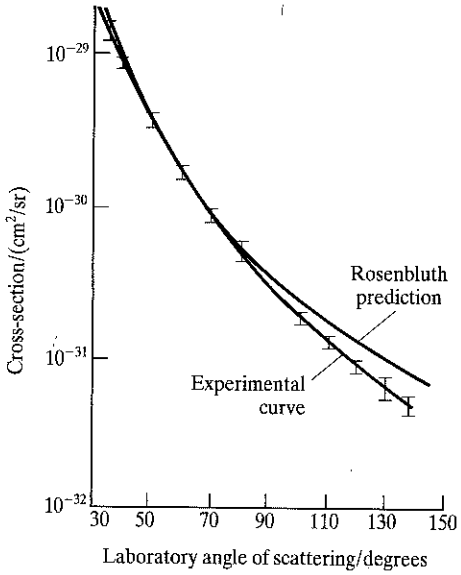

Figure 12.3 Differential cross-section for the elastic scattering of 188 MeV electrons from hydrogen (after Hofstadter R and McAllister R W 1955 *Phys Rev* **98** (217)).

inelastic scattering region. In this region the differential cross-sections for electron scattering are consistent with the picture that the scattering is due to point-like *partons*, constituent parts of the nucleon. In section 12.5 we will show that the properties of the partons are precisely those of the quarks discussed in chapter 10.

High energy muons and neutrinos have also been used to study hadron structure; like electrons they are believed to be structureless and free from complexity due to the strong interaction. Moreover, the coupling of electrons and muons to the electromagnetic field is well understood and cross-sections should therefore be exactly calculable. We illustrate this in principle in the following section.

12.2 *Elastic electron–muon scattering*

Elastic electron–muon scattering

$$e^- + \mu^- \rightarrow e^- + \mu^-$$

$$1 + 2 \rightarrow 3 + 4$$

is dominated by single photon exchange and is therefore described by the Feynman diagram shown in figure 12.4.

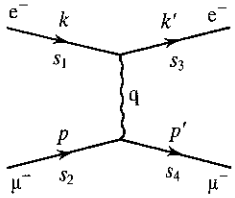

Figure 12.4
Feynman diagram for lowest-order e–μ scattering.

The invariant amplitude for this process is

$$\mathcal{M}_{fi} = [\bar{u}(k')\gamma^\mu u(k)]\frac{e^2}{q^2}[\bar{u}(p')\gamma_\mu u(p)] \qquad (12.7)$$

where $\bar{u}(k')\gamma^\mu u(k)$, for example, is the (vector) electromagnetic current of the electron and $q = (k - k')$ is the exchanged four-momentum (see section 11.5.1). For unpolarized initial and final states an average over initial and sum over final spin states is performed to give the spin-averaged amplitude

$$\begin{aligned}|\overline{\mathcal{M}_{fi}}|^2 &= \frac{1}{4}\sum_{s_1 s_2 s_3 s_4}\left|\bar{u}(k', s_3)\gamma^\mu u(k, s_1)\frac{e^2}{q^2}\bar{u}(p', s_4)\gamma_\mu u(p, s_2)\right|^2 \\ &= \frac{e^4}{4q^4}\sum_{s_1 s_2 s_3 s_4}[\bar{u}(k', s_3)\gamma^\mu u(k, s_1)][\bar{u}(p', s_4)\gamma_\mu u(p, s_2)] \\ &\quad \times [\bar{u}(k', s_3)\gamma^\nu u(k, s_1)]^*[\bar{u}(p', s_4)\gamma_\nu u(p, s_2)]^* \qquad (12.8)\end{aligned}$$

where s_i is the spin component of particle i. Equation (12.8) may be

written

$$|\mathscr{M}_{fi}|^2 = \frac{e^4}{4q^4} L^{\mu\nu}_{(e)} L^{(\mu)}_{\mu\nu} \tag{12.9}$$

where the electron tensor

$$L^{\mu\nu}_{(e)} = \sum_{s_1 s_3} [\bar{u}(k', s_3)\gamma^\mu u(k, s_1)][\bar{u}(k', s_3)\gamma^\nu u(k, s_1)]^* \tag{12.10}$$

with a similar expression for the muon tensor $L^{(\mu)}_{\mu\nu}$. In order to evaluate (12.10) we note that $[\bar{u}(k', s_3)\gamma^\nu u(k, s_1)]$ is just a complex number, a 1×1 matrix, so that taking its complex conjugate is equivalent to taking its hermitian conjugate. Thus

$$\begin{aligned}[\bar{u}(k', s_3)\gamma^\nu u(k, s_1)]^* &= [u^\dagger(k', s_3)\gamma^0\gamma^\nu u(k, s_1)]^* \\ &= [u^\dagger(k, s_1)\gamma^{\nu\dagger}\gamma^0 u(k', s_3)] \\ &= [u^\dagger(k, s_1)\gamma^0\gamma^\nu u(k', s_3)] \\ &= [\bar{u}(k, s_1)\gamma^\nu u(k', s_3)].\end{aligned}$$

In the penultimate step we have used the fact that $\gamma^{\nu\dagger}\gamma^0 = \gamma^0\gamma^\nu$ for,

with $\nu = 0$ $\quad \gamma^{0\dagger}\gamma^0 = \gamma^0\gamma^0$

and

with $\nu = i = 1, 2, 3$ $\quad \gamma^{i\dagger}\gamma^0 = -\gamma^i\gamma^0 = \gamma^0\gamma^i$.

Then,

$$L^{\mu\nu}_{(e)} = \sum_{s_1 s_3} \bar{u}(k', s_3)\gamma^\mu u(k, s_1)\bar{u}(k, s_1)\gamma^\nu u(k', s_3). \tag{12.11}$$

The evaluation of this expression is facilitated by writing the matrix indices explicitly; the usual summation over repeated indices is implied. Thus,

$$L^{\mu\nu}_{(e)} = \sum_{s_3} \bar{u}_\alpha(k', s_3)(\gamma^\mu)_{\alpha\beta} \sum_{s_1} u_\beta(k, s_1)\bar{u}_\gamma(k, s_1)(\gamma^\nu)_{\gamma\delta} u_\delta(k', s_3).$$

Now

$$\sum_{s_1} u_\beta(k, s_1)\bar{u}_\gamma(k, s_1) = (\not{k} + m)_{\beta\gamma}$$

by the completeness relation for Dirac spinors (see appendix K). Here, we have introduced the notation $\gamma^\mu a_\mu \equiv \not{a}$, where a is a four-vector. Then

$$L^{\mu\nu}_{(e)} = \sum_{s_3} \bar{u}_\alpha(k', s_3)(\gamma^\mu)_{\alpha\beta}(\not{k} + m)_{\beta\gamma}(\gamma^\nu)_{\gamma\delta} u_\delta(k', s_3).$$

Since the matrix elements are just numbers their order is unimportant so that

$$L^{\mu\nu}_{(e)} = \sum_{s_3} u_\delta(k', s_3)\bar{u}_\alpha(k', s_3)(\gamma^\mu)_{\alpha\beta}(\not{k} + m)_{\beta\gamma}(\gamma^\nu)_{\gamma\delta}$$
$$= (\not{k}' + m)_{\delta\alpha}(\gamma^\mu)_{\alpha\beta}(\not{k} + m)_{\beta\gamma}(\gamma^\nu)_{\gamma\delta}$$
$$= \mathrm{Tr}[(\not{k}' + m)\gamma^\mu(\not{k} + m)\gamma^\nu]. \tag{12.12}$$

Here, m is the electron mass.

Similarly, the muon tensor becomes

$$L^{(\mu)}_{\mu\nu} = \mathrm{Tr}[(\not{p}' + M)\gamma_\mu(\not{p} + M)\gamma_\nu] \tag{12.13}$$

where M is the muon mass.

The problem is thus reduced to the evaluation of traces and this is readily achieved by making use of the trace theorems proved in appendix L. We have

$$L^{\mu\nu}_{(e)} = \mathrm{Tr}[\not{k}'\gamma^\mu\not{k}\gamma^\nu] + m\,\mathrm{Tr}[\gamma^\mu\not{k}\gamma^\nu] + m\,\mathrm{Tr}[\not{k}'\gamma^\mu\gamma^\nu] + m^2\,\mathrm{Tr}[\gamma^\mu\gamma^\nu].$$

The terms $m\,\mathrm{Tr}[\gamma^\mu\not{k}\gamma^\nu]$ and $m\,\mathrm{Tr}[\not{k}'\gamma^\mu\gamma^\nu]$ are both zero because they contain an odd number of γ matrices. Then,

$$L^{\mu\nu}_{(e)} = \mathrm{Tr}[\not{k}'\gamma^\mu\not{k}\gamma^\nu] + 4m^2g^{\mu\nu}$$

by theorem (iii) of appendix L. We can evaluate the first term by multiplying by two arbitrary four-vectors a and b and noting that

$$a_\mu b_\nu\,\mathrm{Tr}[\not{k}'\gamma^\mu\not{k}\gamma^\nu] = \mathrm{Tr}[\not{k}'\not{a}\not{k}\not{b}].$$

Using theorem (vii) of appendix L we have

$$\mathrm{Tr}[\not{k}'\not{a}\not{k}\not{b}] = 4[(k'\cdot a)(k\cdot b) + (k'\cdot b)(k\cdot a) - (k'\cdot k)(a\cdot b)]$$
$$= 4a_\mu b_\nu[k'^\mu k^\nu + k'^\nu k^\mu - (k'\cdot k)g^{\mu\nu}].$$

Thus,

$$\mathrm{Tr}[\not{k}'\gamma^\mu\not{k}\gamma^\nu] = 4[k'^\mu k^\nu + k'^\nu k^\mu - (k'\cdot k)g^{\mu\nu}]$$

and therefore,

$$L^{\mu\nu}_{(e)} = 4[k'^\mu k^\nu + k'^\nu k^\mu + (m^2 - k'\cdot k)g^{\mu\nu}]. \tag{12.14}$$

The corresponding expression for the muon is

$$L^{(\mu)}_{\mu\nu} = 4[p'_\mu p_\nu + p'_\nu p_\mu + (M^2 - p'\cdot p)g_{\mu\nu}]. \tag{12.15}$$

On forming the product of the electron and muon tensors we find that the spin-averaged invariant amplitude is finally

$$\overline{|\mathcal{M}_{fi}|^2} = \frac{8e^4}{q^4}[(k'\cdot p')(k\cdot p) + (k'\cdot p)(k\cdot p') - m^2(p'\cdot p) - M^2(k'\cdot k) + 2m^2M^2]. \tag{12.16}$$

To arrive at our stated goal of deriving equation (12.6) let us evaluate this expression in the 'laboratory' frame, i.e. the frame in which the muon is at rest. If we neglect terms involving the electron mass we have

$$\overline{|\mathcal{M}_{fi}|^2} = \frac{8e^4}{q^4}[(k'\cdot p')(k\cdot p) + (k'\cdot p)(k\cdot p') - M^2(k'\cdot k)]. \tag{12.17}$$

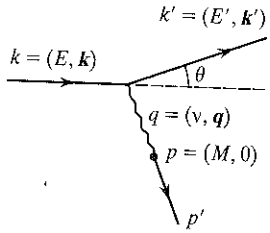

Figure 12.5
Definition of kinematic variables in e–μ scattering in the muon rest frame.

The kinematic variables in the laboratory frame are shown in figure 12.5. It is evident that the four-momentum transfer is $q = k - k' = p' - p$ and therefore $p' = k - k' + p$. On eliminating p' (see example 12.1) the invariant amplitude becomes

$$\overline{|\mathcal{M}_{fi}|^2} = \frac{8e^4}{q^4}[-\tfrac{1}{2}q^2(k\cdot p - k'\cdot p) + 2(k'\cdot p)(k\cdot p) + \tfrac{1}{2}M^2q^2]. \tag{12.18}$$

When expressed in terms of the directly measurable quantities E, E' and θ, equation (12.18) becomes (see example 12.2)

$$\overline{|\mathcal{M}_{fi}|^2} = \frac{8e^4}{q^4}2EE'M^2\left[\cos^2\left(\frac{\theta}{2}\right) - \frac{q^2}{2M^2}\sin^2\left(\frac{\theta}{2}\right)\right]. \tag{12.19}$$

When this matrix element and the Lorentz invariant phase space factor are used in Fermi's golden rule we obtain the differential cross-section for the scattering of an electron into solid angle $d\Omega$ with energy in the range E' to $E' + dE'$:

$$\frac{d^2\sigma}{d\Omega\, dE'} = \frac{4\alpha^2E'^2}{q^4}\left[\cos^2\left(\frac{\theta}{2}\right) - \frac{q^2}{2M^2}\sin^2\left(\frac{\theta}{2}\right)\right]\delta\left(\nu + \frac{q^2}{2M}\right). \tag{12.20}$$

After integration over E' (see, for example, reference 4 for details) we obtain

$$\frac{d\sigma}{d\Omega} = \frac{\alpha^2}{4E^2\sin^4(\theta/2)}\frac{1}{1 + (2E/M)\sin^2(\theta/2)} \times\left[\cos^2\left(\frac{\theta}{2}\right) - \frac{q^2}{2M^2}\sin^2\left(\frac{\theta}{2}\right)\right]. \tag{12.21}$$

This may be rewritten in the form

$$\frac{d\sigma}{d\Omega} = \left(\frac{d\sigma}{d\Omega}\right)_{\text{Mott}} \left[1 - \frac{q^2}{2M^2} \tan^2\left(\frac{\theta}{2}\right)\right] \tag{12.22}$$

where

$$\left(\frac{d\sigma}{d\Omega}\right)_{\text{Mott}} = \frac{\alpha^2 \cos^2(\theta/2)}{4E^2 \sin^4(\theta/2)[1 + (2E/M)\sin^2(\theta/2)]}. \tag{12.23}$$

Equation (12.22) plays an important role in the study of the structure of the proton through e–p scattering. The $\sin^2(\theta/2)$ term in this equation arises from scattering from the magnetic moment of the muon.

12.3 *Elastic electron–proton scattering*

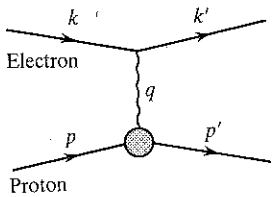

Figure 12.6
Feynman diagram for elastic e–p scattering.

Elastic electron–proton scattering, like elastic electron–muon scattering, is dominated by single photon exchange as shown in figure 12.6. The main difference between these two processes is that, unlike the known photon–muon coupling, the photon–proton coupling is unknown. We can, nevertheless, use the electron–muon calculation of the previous section as a model.

The invariant amplitude takes the same form, namely

$$\mathcal{M}_{fi} = j_\mu \frac{1}{q^2} J^\mu.$$

As before, the electron current is given by

$$j_\mu = -e\bar{u}(k')\gamma_\mu u(k)$$

but the proton current J^μ must reflect the complex proton structure. The proton spinors $\bar{u}(p')$ and $u(p)$ satisfy the Dirac equation and the proton electromagnetic current will have the form

$$J^\mu = e\bar{u}(p')\Gamma^\mu u(p).$$

J^μ must be a Lorentz four-vector and the most general form which satisfies this condition is[5]

$$\Gamma^\mu = \left[F_1(q^2)\gamma^\mu + \frac{\kappa}{2m} F_2(q^2) i\sigma^{\mu\nu} q_\nu\right]$$

where $\sigma^{\mu\nu} = (i/2)[\gamma^\mu, \gamma^\nu]$ and $F_1(q^2)$, $F_2(q^2)$ are two independent form factors. The quantity κ ($=1.79$ nuclear magnetons) is the anomalous part of the magnetic moment of the proton and, of course, m is now the mass of the proton. In the limit $q^2 \to 0$, the virtual photon has a very long wavelength and is insensitive to the structure of the proton which therefore appears to be a particle with charge e and magnetic moment $(1 + \kappa)e/2m$. The form factors in this limit must therefore have the values $F_1(0) = 1$ and $F_2(0) = 1$.

In calculating the differential cross-section the electron tensor $L^{(e)}_{\mu\nu}$ is as before but the proton tensor

$$W^{\mu\nu} = \mathrm{Tr}[(\not{p}' + m)\Gamma^\mu(\not{p} + m)\Gamma^\nu]$$

replaces the muon tensor $L^{\mu\nu}_{(\mu)}$. With this modification the calculation proceeds as before with the result

$$\frac{d\sigma}{d\Omega} = \left(\frac{d\sigma}{d\Omega}\right)_{\text{Mott}} \left\{ \left[F_1^2(q^2) - \frac{\kappa^2 q^2}{4m^2} F_2^2(q^2) \right] - \frac{q^2}{2m^2}[F_1(q^2) + \kappa F_2(q^2)]^2 \tan^2\left(\frac{\theta}{2}\right) \right\}. \tag{12.24}$$

This is the Rosenbluth formula, with $(d\sigma/d\Omega)_{\text{Mott}}$ given by equation (12.23). If the proton were structureless like the muon, κ would be zero and $F_1(q^2)$ would be unity for all values of q^2; the Rosenbluth formula would then revert to equation (12.22). As it stands, equation (12.24) contains an interference term between F_1 and F_2 and it is conventional to define the electric and magnetic form factors of the proton as

$$G_E = F_1 + \frac{\kappa q^2}{4m^2} F_2$$

$$G_M = F_1 + \kappa F_2.$$

In the limit $q^2 \to 0$, $G_E(0) = 1$ and $G_M(0) = 1 + \kappa = \mu_p$, the magnetic moment of the proton. In terms of these form factors the interference term disappears and the expression for the differential cross-section becomes

$$\frac{d\sigma}{d\Omega} = \left(\frac{d\sigma}{d\Omega}\right)_{\text{Mott}} \left[\frac{G_E^2 - (q^2/4m^2)G_M^2}{1 - q^2/4m^2} - \frac{q^2}{2m^2} G_M^2 \tan^2\left(\frac{\theta}{2}\right) \right]. \tag{12.25}$$

The electric and magnetic form factors for the proton can thus be determined by comparing the differential cross-section for elastic electron–proton scattering, measured in the laboratory system, with that expected on the basis of the Mott formula. In practice, equation (12.25) is often

rewritten with $Q^2 = -q^2$ so that

$$\frac{\mathrm{d}\sigma/\mathrm{d}\Omega}{(\mathrm{d}\sigma/\mathrm{d}\Omega)_{\mathrm{Mott}}} = A(Q^2) + B(Q^2)\tan^2\left(\frac{\theta}{2}\right)$$

where

$$A = \frac{G_{\mathrm{E}}^2 + (Q^2/4m^2)G_{\mathrm{M}}^2}{1 + Q^2/4m^2} \qquad B = \frac{Q^2 G_{\mathrm{M}}^2}{2m^2}.$$

The form factors G_{E} and G_{M} can then be determined by performing a series of experiments at different values of q^2 at each of which $\mathrm{d}\sigma/\mathrm{d}\Omega$ is measured as a function of θ. For a given fixed q^2, figure 12.7 shows a typical dependence of $(\mathrm{d}\sigma/\mathrm{d}\Omega)/(\mathrm{d}\sigma/\mathrm{d}\Omega)_{\mathrm{Mott}}$ on $\tan^2(\theta/2)$. The experimental observation of a linear dependence on $\tan^2(\theta/2)$ validates the assumption of single photon exchange as the dominant mechanism in elastic electron–proton scattering. The magnetic form factor at a particular value of q^2 is determined directly from the slope of the graph and, using this value of $G_{\mathrm{M}}(q^2)$, $G_{\mathrm{E}}(q^2)$ is determined from the intercept.

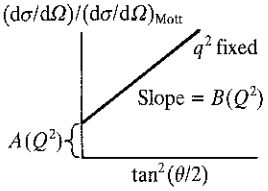

Figure 12.7. Graph showing the linear relationship between $(\mathrm{d}\sigma/\mathrm{d}\Omega)/(\mathrm{d}\sigma/\mathrm{d}\Omega)_{\mathrm{Mott}}$ and $\tan^2(\theta/2)$ at a fixed value of q^2.

Because free neutron targets are not available, deuterium or heavier nuclei have to be used to measure the neutron form factor. Because of its low binding energy and relatively simple structure, deuterium is a natural choice. Nonetheless, in analysing electron–deuteron scattering, complications do arise from the nuclear physics of the deuteron.

Typical results[6] for the form factors of the proton and neutron are shown in figure 12.8. It is found that they satisfy a simple *scaling*

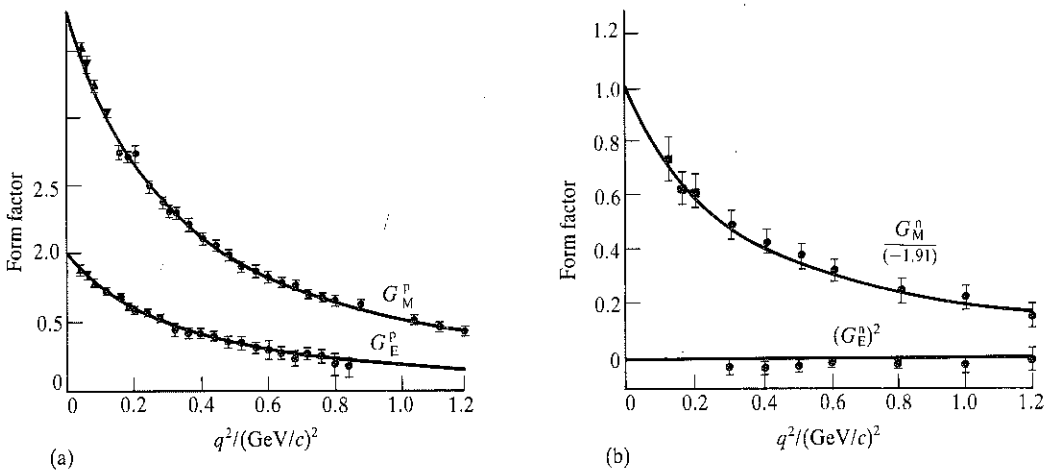

Figure 12.8 Electric and magnetic form factors as a function of q^2 for (a) the proton and (b) the neutron. (After Hughes E B *et al.* 1965 *Phys Rev* **139B** (458).)

law

$$G_E^p(q^2) = \frac{G_M^p(q^2)}{\mu_p} = \frac{G_M^n(q^2)}{\mu_n} \qquad G_E^n(q^2) = 0 \tag{12.26}$$

and are well described by the *dipole formula*

$$G(q^2) = \left(1 - \frac{q^2}{m^2}\right)^{-2}$$

with $m^2 = 0.71\ \text{GeV}^2$. It is straightforward to show that these form factors correspond to a charge (and magnetic moment) distribution of the form $\rho \approx \exp(-mr)$ with a root-mean-square radius of 0.8 fm (see examples 12.3 and 12.4).

12.4 *Inelastic electron–proton scattering*

At large values of q^2 the elastic cross-section is very small and inelastic scattering becomes much more probable. We shall consider the process $ep \rightarrow eX$, where X is any system of hadrons. For relatively small values of q^2 the proton may merely be excited into a resonant state which then decays into a nucleon and a pion for example. At higher values of q^2 the energy transferred to the proton may be so great that it breaks up into many hadrons and loses its identity completely.

We assume that, as in the case of elastic scattering, single photon exchange is the dominant mechanism. The Feynman diagram describing the process is shown in figure 12.9. Experimentally, the hadronic system

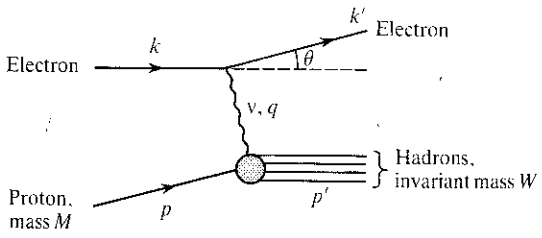

Figure 12.9
Feynman diagram for inelastic e–p scattering.

is disregarded and measurements are made on the scattered electron only. Specifically, the event rate and electron energy for electrons scattered through some angle θ with respect to the incident beam direction are measured. The cross-section measured in this way is called the 'inclusive' cross-section.

In the case of elastic scattering the energy transfer ν and the four-momentum transfer q^2 are related by the expression $\nu = -q^2/2M$ and are thus not independent variables. In contrast, in inelastic scattering ν and q^2 are *independent* scalar variables. For, from conservation of energy and momentum at the hadron vertex in figure 12.9, we have

$$p' = p + q$$

and therefore

$$p'^2 = p^2 + 2p\cdot q + q^2.$$

Now p'^2 is just the invariant mass squared, W^2 say, of the hadronic system. Further, $p\cdot q = M\nu$ and, defining $-q^2 = Q^2$, we have

$$Q^2 = 2M\nu + M^2 - W^2.$$

Since the invariant mass of the hadron system can vary, Q^2 (and hence q^2) and ν are independent variables in inelastic electron–proton scattering.

In analogy with equation (12.24) or equation (12.25) the differential cross-section for the inelastic scattering of an electron with energy in the range E' to $E' + \mathrm{d}E'$ into the solid angle $\mathrm{d}\Omega$ is

$$\frac{\mathrm{d}^2\sigma}{\mathrm{d}\Omega\,\mathrm{d}E'} = \frac{4\alpha^2E'^2}{Q^4}\left[W_2(Q^2,\nu)\cos^2\left(\frac{\theta}{2}\right) + 2W_1(Q^2,\nu)\sin^2\left(\frac{\theta}{2}\right)\right]. \tag{12.27}$$

In inelastic scattering the functions $W_1(Q^2, \nu)$ and $W_2(Q^2, \nu)$, which replace the form factors $G_E(q^2)$ and $G_M(q^2)$, are functions of the two independent variables Q^2 and ν. They are commonly called *structure functions*.

It is convenient at this stage to introduce the variable $x = Q^2/2M\nu$ which plays an important role in what follows. In order to gain some familiarity with these variables we show the kinematic relationships between them in figure 12.10.

The condition for elastic scattering is $W = M$, in which case $Q^2 = 2M\nu$ as required. This is a straight line at 45° to the axes as shown in figure 12.10 and corresponds to $x = 1$. The region above this line is kinematically forbidden. Inelastic scattering corresponds to $W^2 > M^2$ and therefore $Q^2 < 2M\nu$, i.e. to the region below the elastic scattering line. The lines drawn parallel to the line $x = 1$ correspond to the production of a hadron system with a fixed invariant mass W and may, for instance, represent the electroproduction of a nucleon resonance. The line corresponding to the production of a resonance with mass W' intercepts the horizontal axis at $2M\nu = W'^2 - M^2$. From the definition of x we have $Q^2 = x2M\nu$ and therefore lines of constant x pass through the origin and have slope x.

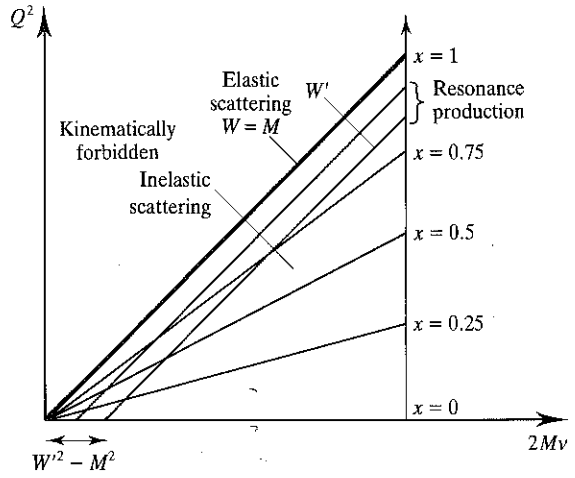

Figure 12.10 Diagram showing the relationship between the kinematic variables Q^2 and v. M is the mass of the proton and W is the mass of the hadronic system produced in the process $ep \rightarrow eX$ (see figure 12.9).

Finally, the region in which both Q^2 and v are large is known as the *deep inelastic* scattering region. Scattering experiments in this region are of the utmost importance for it is here that the internal structure of the proton is revealed; the proton consists of point-like partons.

In order to understand better the arguments on which this latter statement is based we draw on examples from nuclear physics and develop the ideas put forward in section 3.3. Specifically, we consider the scattering of electrons by ^{4}He nuclei and present the data taken at 400 MeV incident electron energy by Hofstadter.[7] Figure 12.11(a) shows the cross-section in arbitrary units for electrons scattered through 45° in the laboratory system plotted as a function of $x = Q^2/2M_\alpha v$, where M_α is the mass of the helium nucleus. At $x \approx 1$ one sees a pronounced peak due to coherent elastic scattering from the helium nucleus. At smaller values of x, i.e. larger values of energy transfer to the nucleus, there is a broad peak due to inelastic scattering. Shown for reference is the elastic scattering peak from free protons which occurs at $x \approx 0.25$. This suggests that the inelastic peak, which is distributed about $x \approx 0.25$, is due to the incoherent elastic scattering from the individual constituents, i.e. the nucleons, in the helium nucleus. The effective mass of each nucleon in ^{4}He will be roughly $m = M_\alpha/4$ so that if elastic scattering is taking place from individual nucleons it should occur at $x = Q^2/2mv$. Hence this quasi-elastic scattering peak should appear at $x = m/M_\alpha \approx 1/N$ where N is the number of constituent nucleons (four in the present case). The quasi-elastic scattering peak is smeared out because the nucleons are not free but are bound inside the nuclear volume and have a Fermi momentum $\Delta p \approx R^{-1}$ where R is the nuclear radius. Figure 12.11(b) shows the cross-section for elastic and inelastic electron–helium scattering again at 400 MeV but at an

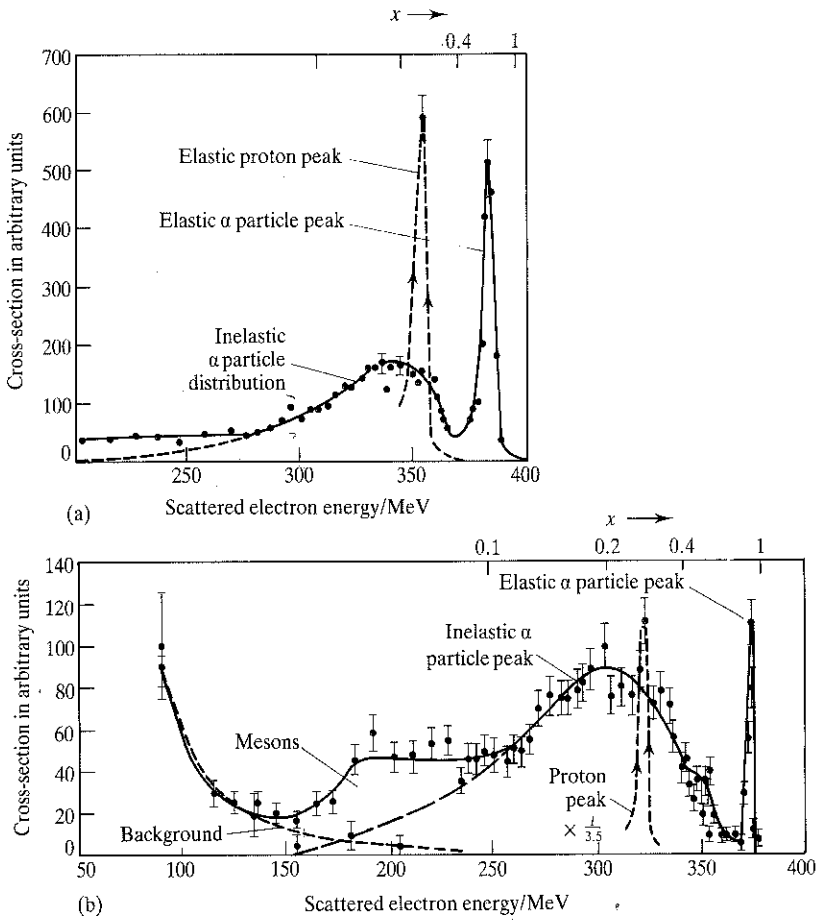

Figure 12.11 Cross-sections for the elastic and inelastic scattering of 400 MeV electrons by ^{4}He nuclei as a function of x. The scattering angle of the electrons in the laboratory system is 45° in part (a) and 60° in part (b). (After Hofstadter R 1956 *Rev Mod Phys* **28** (214).)

increased scattering angle of 60°. This corresponds to a higher value of Q^2. The first point to notice is that the elastic e–α cross-section is much reduced at this higher value of Q^2; the cross-section is suppressed by the form factor. On the other hand, the quasi-elastic scattering from the individual nucleons is essentially independent of Q^2; the cross-section is said to *scale*. This behaviour is typical for scattering from a point-like or structureless particle.

To gain some insight into this scaling behaviour consider a dipole form factor $F(Q^2) = 1/(1 + Q^2/\Lambda^2_{\text{nuc}})^2$. In this expression Λ_{nuc} sets a scale and the behaviour of the cross-section (through the form factor) depends on the relative values of Q^2 and the scale Λ^2_{nuc}. For $Q^2 \ll \Lambda^2_{\text{nuc}}$, $F(Q^2) \to 1$. In this situation the electromagnetic probe has a very long wavelength

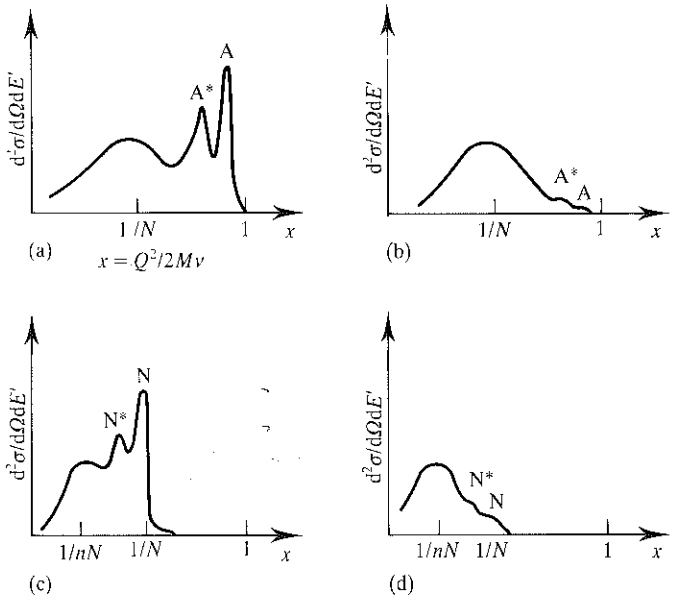

Figure 12.12 Schematic diagram showing the development of the scattering cross-section for electrons on a hypothetical nucleus A, as a function of x, as Q^2 increases. (a) The pronounced peaks are due to elastic scattering, eA → eA, at $x \approx 1$ and formation of excited nuclear states A*. The broad peak, due to quasi-elastic scattering from individual nucleons, is centred around $x = 1/N$, where N is the number of nucleons in the nucleus, and is smeared due to Fermi motion. (b) At higher values of Q^2 the elastic peaks become much reduced due to the nuclear form factor but the quasi-elastic scattering peak is virtually unaffected; it scales. (c) At still higher values of Q^2 the nucleon constituents are revealed. The pronounced peaks are due to elastic e–N scattering and formation of excited nucleon states N*. The quasi-elastic scattering peak is centred around $x = 1/nN$ where n is the number of nucleon constituents. Fermi motion of the nucleon constituents smears out this peak. (d) As Q^2 increases further the only remaining feature is the quasi-elastic scattering from the nucleon constituents; this cross-section scales.

compared with the scale and is therefore insensitive to the detailed internal structure of the target; scattering takes place as if from a point. As Q^2 increases the elastic cross-section decreases. There is a different scale, Λ_{nucleon}, for the nucleons but provided $Q^2 \ll \Lambda^2_{\text{nucleon}}$ no internal structure of the nucleons will be revealed and quasi-elastic scattering will take place from the nucleons as though they were point-like; the quasi-elastic e–nucleon scattering is scale invariant – the cross-section scales. The quasi-elastic peak will occur at $x \approx 1/N$ where N is the number of nucleon constituents and it will be spread out due to the Fermi motion of the nucleons inside the nucleus. One can imagine continuing this process to investigate the substructure of the nucleons themselves. Suppose for the sake of argument there is another, perhaps ultimate, scale Λ_0. As Q^2 increases beyond $\Lambda^2_{\text{nucleon}}$ the elastic e–α peak will tend to disappear, the quasi-elastic scattering peak will become reduced due to the form factor of the nucleon and quasi-elastic scattering from the nucleon constituents will set in. If there are n nucleon constituents the quasi-elastic scattering

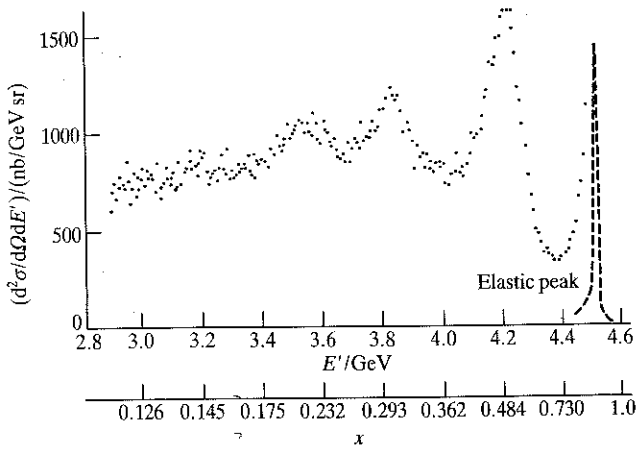

Figure 12.13 Differential cross-section for e–p scattering at 10° as a function of E', the energy of the scattered electron in the laboratory system, and x. The elastic peak at $x = 1$ has been reduced by a factor of 15. The incident beam energy was 4.879 GeV. (After Bartel W *et al.* 1968 *Phys Lett* **28B** (148).)

from these will appear at $x \approx 1/nN$ and again will be smeared out due to Fermi motion. The cross-section for this quasi-elastic scattering from the nucleon constituents will remain constant as Q^2 is increased further and if indeed there is no other scale, $\Lambda < \Lambda_0$, the constancy of the cross-section would indicate a lack of any further substructure. This phenomenon of scaling and rescaling as Q^2, and hence the resolution, increases to reveal deeper and deeper levels of matter is summarized in figure 12.12. Note the gradual shift of the quasi-elastic scattering peak to lower and lower values of x as more and more constituents are revealed.

Consider now the scattering of electrons from hydrogen. In figure 12.13 we show results from the electron synchrotron at DESY obtained by Bartel *et al.*[8] These data are at much higher values of Q^2 than the electron–helium data but the similarity between figure 12.11 and figure 12.13 is unmistakable. A large peak due to elastic e–p scattering is clearly visible at $x = 1$, as are peaks at lower x values corresponding to the excitation of nucleon resonances through the processes

$$\mathrm{e} + \mathrm{p} \rightarrow \begin{cases} \mathrm{e} + \Delta(1232) \\ \mathrm{e} + \mathrm{N}(1450) \\ \mathrm{e} + \Delta(1688). \end{cases}$$

Beyond the resonances, at higher energy transfers to the nucleon (lower values of x) there is a broad continuum which, in analogy with the case of electron–helium scattering, is interpreted as quasi-elastic scattering from the nucleon constituents. The absence of a peak in this region is due to the Fermi motion of the constituents. At higher values of Q^2 the elastic

and resonance peaks decrease due to the fall-off in the form factors but the quasi-elastic scattering is virtually unaffected – the cross-section scales indicating scattering from point-like constituents.

12.5 *Bjorken scaling and the parton model*

In this section we develop further our investigation into the structure of the proton and to this end we begin by collecting together the relevant pieces of formalism presented earlier in this chapter.

The differential cross-sections for the processes discussed so far may all be expressed in the form

$$\frac{\mathrm{d}^2\sigma}{\mathrm{d}\Omega\,\mathrm{d}E'} = \frac{4\alpha^2 E'^2}{Q^4} S$$

where S in general represents the structure, if any, of the target particle. For example, the differential cross-section for elastic e–μ scattering, in which both the electron and muon are structureless, is given by equation (12.20) and

$$S_{e\mu\to e\mu} = \left[\cos^2\left(\frac{\theta}{2}\right) + \frac{Q^2}{2M^2}\sin^2\left(\frac{\theta}{2}\right)\right]\delta\left(\nu - \frac{Q^2}{2M}\right). \tag{12.28}$$

In this expression M is the mass of the muon. The presence of the δ function merely stresses the fact that in elastic scattering the energy transfer ν and the four-momentum transfer Q^2 are not independent; they are related by the equation $\nu = Q^2/2M$.

In contrast, in inelastic scattering Q^2 and ν are independent variables, and the differential cross-section for the inelastic process $ep \to eX$, see equation (12.27), has

$$S_{ep\to eX} = W_2(Q^2, \nu)\cos^2\left(\frac{\theta}{2}\right) + 2W_1(Q^2, \nu)\sin^2\left(\frac{\theta}{2}\right). \tag{12.29}$$

The complex structure of the proton is reflected in the presence of the two structure functions W_1 and W_2 which, for values of Q^2 less than about 1 $(\mathrm{GeV}/c)^2$, are functions of both Q^2 and ν.

In the last section we presented evidence which pointed to the existence of point-like constituents (partons) in the proton. A natural guess would be that these partons are in fact the spin $\frac{1}{2}$ quarks. If, at high values of Q^2, the virtual photon does indeed elastically scatter from an essentially free spin $\frac{1}{2}$ quark, expression (12.29), which describes the proton structure, should reduce to (12.28) which describes elastic scattering from a

structureless spin $\frac{1}{2}$ Dirac particle – the muon. Comparison of (12.29) and (12.28) shows that if inelastic e–p scattering is an *incoherent* superposition of elastic scattering from quarks the proton structure functions should reduce to the point form

$$2W_1 = \frac{Q^2}{2m^2}\,\delta\left(\nu - \frac{Q^2}{2m}\right) \tag{12.30}$$

$$W_2 = \delta\left(\nu - \frac{Q^2}{2m}\right) \tag{12.31}$$

where m is the quark mass. If we make use of the property $\delta(ax) = a^{-1}\delta(x)$, (12.30) and (12.31) may be rewritten as

$$2mW_1(Q^2, \nu) = \frac{Q^2}{2m\nu}\,\delta\left(1 - \frac{Q^2}{2m\nu}\right) \tag{12.32}$$

$$\nu W_2(Q^2, \nu) = \delta\left(1 - \frac{Q^2}{2m\nu}\right). \tag{12.33}$$

These point 'structure functions' have the remarkable property that the independent variables Q^2 and ν appear only in the dimensionless ratio $x = Q^2/2m\nu$; the structure functions are no longer functions of Q^2 and ν separately. This phenomenon is known, somewhat paradoxically, as Bjorken scaling. Its occurrence would signal the fact that, as Q^2 increases into the deep inelastic region and the wavelength of the virtual photon becomes shorter and shorter, elastic scattering from the proton, which may be regarded as due to the *coherent* action of all the quarks inside the proton, is replaced by an *incoherent* superposition of elastic scattering from individual point-like quarks.

To stress that there is *no* scale of mass or length in this deep inelastic region let us consider again elastic e–p scattering. From equation (12.25) we have

$$S_{ep\to ep} = \left[\frac{G_E^2 + \tau G_M^2}{1+\tau}\cos^2\left(\frac{\theta}{2}\right) + 2\tau G_M^2 \sin^2\left(\frac{\theta}{2}\right)\right]\delta\left(\nu - \frac{Q^2}{2M}\right) \tag{12.34}$$

where $\tau = Q^2/4M^2$ and M is now the proton mass. Let us simplify this expression by assuming that the proton does not possess an anomalous magnetic moment. Then, $G_E = G_M = G(Q^2)$, say, and (12.34) becomes

$$S_{ep\to ep} = G^2(Q^2)\left[\cos^2\left(\frac{\theta}{2}\right) + \frac{Q^2}{2M^2}\sin^2\left(\frac{\theta}{2}\right)\right]\delta\left(\nu - \frac{Q^2}{2M}\right). \tag{12.35}$$

On comparing this expression with (12.29) we can write the elastic

structure functions of the proton as

$$W_1(Q^2, \nu) = G^2(Q^2)\frac{Q^2}{4M^2}\delta\left(\nu - \frac{Q^2}{2M}\right)$$
$$W_2(Q^2, \nu) = G^2(Q^2)\delta\left(\nu - \frac{Q^2}{2M}\right). \tag{12.36}$$

Because of the presence of the form factor $G(Q^2)$ these expressions cannot be rewritten as functions of the dimensionless variable x. We saw in section 12.3 that the form factors are well described by the dipole formula

$$G(Q^2) = \left(1 + \frac{Q^2}{m^2}\right)^{-2}$$

in which the *mass scale* is determined experimentally to be $m^2 = 0.71\ \text{GeV}^2$. In deep inelastic scattering there is no such mass scale.

In summary, the Bjorken scaling hypothesis may be stated as follows: in the limit $Q^2 \to \infty$, $\nu \to \infty$, with $x = Q^2/2M\nu$ fixed, the structure functions scale as

$$MW_1(Q^2, \nu) \to F_1(x) \tag{12.37}$$
$$\nu W_2(Q^2, \nu) \to F_2(x). \tag{12.38}$$

Experimental support for this scaling hypothesis is given in figures 12.14 and 12.15. In figure 12.14 we show the results in inelastic e–p scattering obtained at SLAC by Miller *et al.*[9] The two structure functions are plotted against $\omega = 1/x$ for different values of $Q^2 > 1\ (\text{GeV}/c)^2$. To ensure that the continuum region is being probed, the data are restricted to hadron masses $M_X > 2.6$ GeV, i.e. well away from the resonance region. Within experimental errors, both $2MW_1$ and νW_2 scale: they are functions of x only. Figure 12.15 shows data from Friedman and Kendall[10] for $M_X > 2$ GeV; νW_2 is plotted as a function of Q^2 for the fixed value of $x = 0.25$ and it is seen to be independent of Q^2.

A physical interpretation of Bjorken scaling, and in particular the scaling variable x, was first given by Feynman.[11] Feynman postulated that each parton in the proton carries only a fraction of the energy and momentum of the proton. The scattering process in the deep-inelastic region is visualized as in figure 12.16. The virtual photon, with four-momentum q, is absorbed by a particular parton. Let x be the fraction of the four-momentum of the proton carried by this parton. There are different types of parton (quarks) in the proton so a parton of type i has four-momentum $p_i = xp$ where p is the four-momentum of the proton, and a mass $m_i \approx xM$, M being the proton mass (see example 12.5).

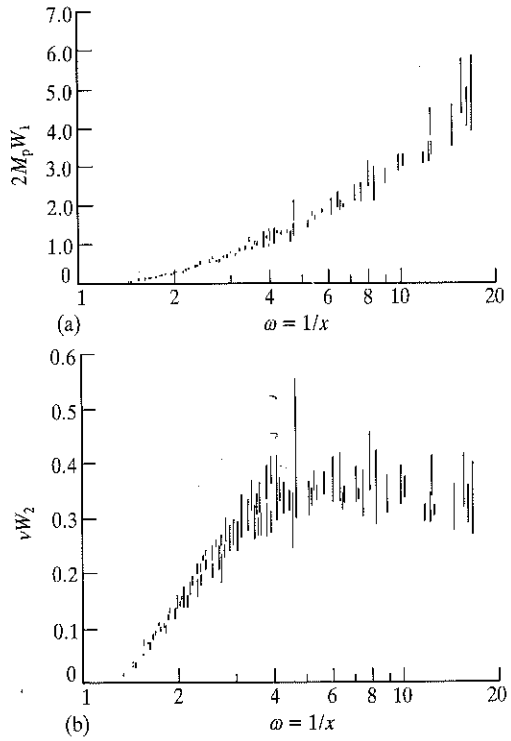

Figure 12.14 Evidence for the scaling of the proton structure functions: (a) $2M_pW_1$ and (b) νW_2 are shown as functions of $\omega = 1/x$ for values of $Q^2 > 1$ (GeV/c)^2. Masses of the hadronic system were required to be greater than 2.6 GeV. (After Miller *G et al.* 1972 *Phys Rev* **D5** (528).)

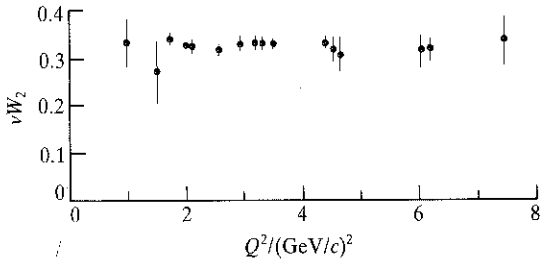

Figure 12.15 The proton structure function νW_2 plotted as a function of Q^2 for the fixed value of $x = 0.25$ and hadron masses greater than 2 GeV. The structure function is independent of Q^2. (After Friedman J I and Kendall H W 1972 *Ann Rev Nucl Sci* **22** (203).)

Assuming, as we are, that the partons are spin $\frac{1}{2}$ quarks, we can write down the differential cross-section for this process by using that for e–μ scattering as a model. The only change in the formula will be the replacement of α by αe_i, where e_i is the fractional charge of quark of type i. Thus, the differential cross-section for elastic scattering of an electron

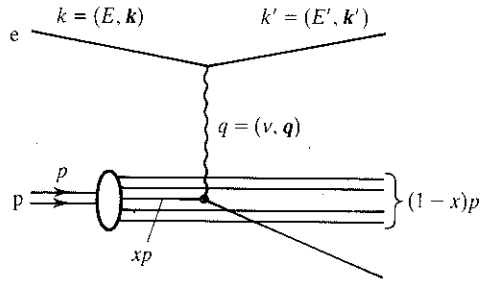

Figure 12.16
Deep inelastic e–p scattering in the parton model.

by a quark of type i becomes

$$\frac{\mathrm{d}^2\sigma^i}{\mathrm{d}\Omega\,\mathrm{d}E'} = \frac{4\alpha^2E'^2}{Q^4}\left[e_i^2\cos^2\left(\frac{\theta}{2}\right) + e_i^2\frac{Q^2}{2m_i^2}\sin^2\left(\frac{\theta}{2}\right)\right]\delta\left(\nu - \frac{Q^2}{2m_i}\right). \tag{12.39}$$

On comparing this with (12.27), the differential cross-section for inelastic e–p scattering, we find, putting $m_i = xM$, that the contribution of parton i to the proton structure functions W_1 and W_2 is

$$W_1^i = e_i^2\frac{Q^2}{4M^2x^2}\,\delta\left(\nu - \frac{Q^2}{2Mx}\right) \tag{12.40}$$

$$W_2^i = e_i^2\,\delta\left(\nu - \frac{Q^2}{2Mx}\right). \tag{12.41}$$

Each parton can, of course, carry a different fraction x of the proton momentum; let $f_i(x)$ be the probability that a parton of type i has momentum fraction x. In the electron–quark scattering process the non-participating partons merely act as 'spectators' so we assume that the contributions of individual quarks to the inelastic e–p differential cross-section add incoherently. We may therefore write

$$W_1(Q^2, \nu) = \sum_i \int e_i^2\frac{Q^2}{4M^2x^2}\,f_i(x)\,\delta\left(\nu - \frac{Q^2}{2Mx}\right)\mathrm{d}x.$$

We integrate this expression using property (iv) of the Dirac δ function given in appendix I and obtain

$$MW_1(Q^2, \nu) = \sum_i \frac{e_i^2}{2}\,f_i(x) \equiv F_1(x) \tag{12.42}$$

with $x = Q^2/2M\nu$. Furthermore,

$$W_2(Q^2, \nu) = \sum_i \int e_i^2 f_i(x)\,\delta\left(\nu - \frac{Q^2}{2Mx}\right)\mathrm{d}x$$

and on performing the integration we get

$$\nu W_2(Q^2, \nu) = \sum_i e_i^2 x f_i(x) \equiv F_2(x). \tag{12.43}$$

It follows that

$$2xF_1(x) = F_2(x). \tag{12.44}$$

This last relation, which is valid only for spin $\frac{1}{2}$ partons, is known as the Callan–Gross[12] relation.

Some insight into the Callan–Gross relation can be obtained from a consideration of the cross-sections for virtual photon–proton interactions. Real photons have $q^2 = 0$ and can exist only in the transverse helicity states $\lambda = \pm 1$, whereas virtual photons have $q^2 < 0$ and can exist in addition in the longitudinal or scalar state with helicity $\lambda = 0$; virtual photons behave like spin 1 particles with non-zero mass. The cross-sections for the production of a hadronic system with mass M_X by transverse and scalar photons are[13]

$$\sigma_T = \frac{4\pi\alpha^2}{K} W_1 \tag{12.45}$$

and

$$\sigma_S = \frac{4\pi\alpha^2}{K}\left[\left(1 + \frac{\nu^2}{Q^2}\right)W_2 - W_1\right]. \tag{12.46}$$

In these expressions K is a flux factor given by $K = (M_X^2 - M^2)/2M$ where M is the proton mass. Since any cross-section must be positive or zero we have

$$W_1 \geqslant 0$$

and

$$\left(1 + \frac{\nu^2}{Q^2}\right)W_2 - W_1 \geqslant 0.$$

In the scaling limit $Q^2 \to \infty$, $\nu \to \infty$ while $x = Q^2/2M\nu$ remains finite, $MW_1(Q^2, \nu) \to F_1(x)$ and $\nu W_2(Q^2, \nu) \to F_2(x)$ so that

$$\sigma_T \to \frac{4\pi\alpha^2}{KM} F_1(x) \tag{12.47}$$

and

$$\sigma_S \to \frac{4\pi\alpha^2}{KM}\frac{1}{2x}[F_2(x) - 2xF_1(x)]. \tag{12.48}$$

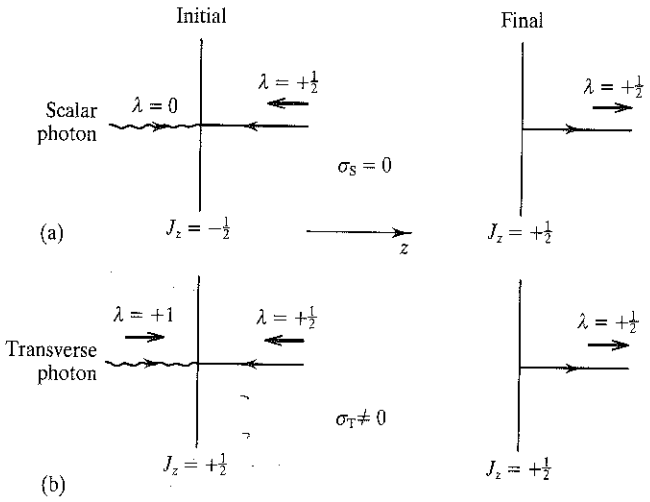

Figure 12.17
Absorption of (a) scalar and (b) transverse photons by helicity conserving partons viewed in the Breit frame of reference.

Let us consider the constraints, if any, imposed on these cross-sections by angular momentum conservation. We work in the Breit frame in which the photon and parton are collinear (see Figure 12.17). On absorption of the photon, the three-momentum of the parton is reversed; momentum is transferred in this frame but not energy. Take the z axis as the direction of the incident photon. In the limit in which its mass may be neglected the parton will have definite helicity, i.e. its component of spin along the direction of motion will be conserved. Figure 12.17(a) shows the absorption of a scalar photon ($\lambda = 0$) by a spin $\frac{1}{2}$ parton with helicity $\lambda = +\frac{1}{2}$. In the initial state the z component of angular momentum is $-\frac{1}{2}$ while in the final state it is $+\frac{1}{2}$. Since angular momentum is not conserved the cross-section for absorption of a scalar photon by a spin $\frac{1}{2}$ parton should be zero. With reference to (12.48) we see that $\sigma_S \to 0$ if $2xF_1 = F_2$, i.e. if the Callan–Gross relation is satisfied. Figure 12.17(b) shows that angular momentum is conserved in the absorption of transverse photons by spin $\frac{1}{2}$ partons; $\sigma_T \neq 0$. Thus, if partons have spin $\frac{1}{2}$, $\sigma_S/\sigma_T \to 0$ and the Callan–Gross relation should be satisfied. On the other hand, partons with spin 0 cannot absorb transverse photons in an angular-momentum-conserving process so that if the partons were spin 0 particles one would expect $\sigma_T/\sigma_S \to 0$. Support for the validity of the Callan–Gross relation and hence for the hypothesis that the partons which interact with the photon, i.e. those which carry electric charge,* have spin $\frac{1}{2}$, is given in figure 12.18.

It is intriguing that the four-momentum fraction x is identical to the dimensionless kinematic variable $x = Q^2/2Mv$ introduced for the virtual

* Here, we are anticipating the existence of gluons. These have spin 1, but, since they are neutral, do not interact with the photon.

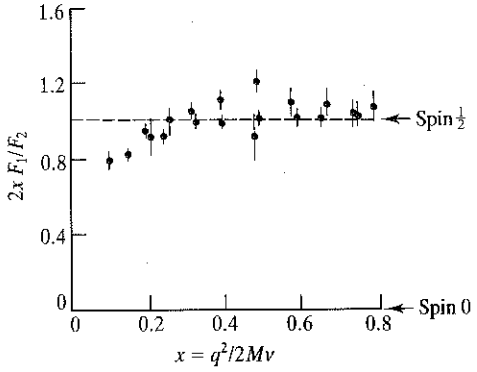

Figure 12.18 Experimental test of the Callan–Gross relation. The data are from a series of e–N scattering experiments performed at the Stanford Linear Accelerator Centre. F_1 and F_2 are extracted from fits to the differential cross-sections in the range $1.5 < q^2 < 16$ GeV^2. For values of $x > 0.2$ the ratio $2xF_1/F_2$ is consistent with unity, the value expected for spin $\frac{1}{2}$ partons.

photon in section 12.4. This means that *in order that the photon be absorbed by a parton with four-momentum x it must have just the right values of Q^2 and ν to give this value of x*. In essence, it is the elastic scattering constraint, $\nu = Q^2/2m_i = Q^2/2Mx$, i.e. $x = Q^2/2M\nu$, which results in the observed scaling behaviour in the deep-inelastic scattering region.

12.6 *Quark structure of the nucleon*

12.6.1 *Electron–nucleon scattering*

The phenomenon of Bjorken scaling embodied in the relations

$$MW_1(Q^2, \nu) \to F_1(x) = \sum_i \frac{e_i^2}{2} f_i(x) \tag{12.49}$$

$$\nu W_2(Q^2, \nu) \to F_2(x) = \sum_i e_i^2 x f_i(x) \tag{12.50}$$

and the experimental evidence in favour of the Callan–Gross relation indicates that the nucleon contains point-like fermion constituents (partons). We associate these partons with the quarks which we saw in chapter 10 were so successful in describing the static properties of the hadrons. The quantum numbers of the proton, for instance, are correctly predicted if one assumes that the proton consists of two u quarks and a d quark. These are known as 'valence' quarks. It should be noted, however, that the same quantum numbers would result if, in addition to the valence

quarks, there exists any number of quark–antiquark pairs $(f, \bar{f})$ so that for any quark flavour f the contribution to the overall quantum numbers of the proton from these pairs is exactly zero. Deep-inelastic scattering experiments point to the existence of these quark–antiquark pairs in addition to the valence quarks; they are known as 'sea' quarks.

Using (12.50) and the quantum numbers of the quarks shown in table 10.2 we may write the structure function F_2^{ep} for electron–proton scattering as

$$F_2^{ep} = x\{\tfrac{4}{9}[u^p(x) + \bar{u}^p(x)] + \tfrac{1}{9}[d^p(x) + \bar{d}^p(x)] + \tfrac{1}{9}[s^p(x) + \bar{s}^p(x)]\}.$$

In this expression $u^p(x)$, for example, is the probability density distribution of u quarks in the proton, $\bar{u}^p(x)$ that for u antiquarks in the proton, etc. We are assuming here that there is negligible contribution from c, b, ... quarks in the proton. Similarly, the structure function for e–n scattering may be written

$$F_2^{en} = x\{\tfrac{4}{9}[u^n(x) + \bar{u}^n(x)] + \tfrac{1}{9}[d^n(x) + \bar{d}^n(x)] + \tfrac{1}{9}[s^n(x) + \bar{s}^n(x)]\}.$$

Now, since the proton and neutron and the u and d quarks form I spin doublets it is expected that

$$\begin{aligned} u^p(x) &= d^n(x) \equiv u(x) \\ d^p(x) &= u^n(x) \equiv d(x) \\ s^p(x) &= s^n(x) \equiv s(x) \end{aligned} \tag{12.51}$$

with similar constraints for the antiquark distribution functions. The e–p and e–n structure functions then become

$$F_2^{ep} = x\{\tfrac{4}{9}[u(x) + \bar{u}(x)] + \tfrac{1}{9}[d(x) + \bar{d}(x)] + \tfrac{1}{9}[s(x) + \bar{s}(x)]\} \tag{12.52}$$

$$F_2^{en} = x\{\tfrac{4}{9}[d(x) + \bar{d}(x)] + \tfrac{1}{9}[u(x) + \bar{u}(x)] + \tfrac{1}{9}[s(x) + \bar{s}(x)]\}. \tag{12.53}$$

We can obtain bounds on the ratio of these structure functions by expressing the quark distribution functions in terms of valence and sea quarks. Thus, in general, we write for any quark flavour q,

$$q(x) = q_v(x) + q_s(x)$$

where the subscripts v and s refer to valence and sea quarks respectively. If the valence quarks in the proton are u_v, u_v and d_v then we have immediately

$$q_v(x) = 0 \qquad \text{for} \qquad q \equiv s, \bar{s}, \bar{u} \text{ and } \bar{d}.$$

The strange quarks and the antiquarks in the proton must belong to the sea. Then,

$$u(x) = u_v(x) + u_s(x)$$

$$d(x) = d_v(x) + d_s(x).$$

If we make the further simplifying assumption that the three light quarks occur in the sea with the same frequency and momentum distributions we have $u_s(x) = d_s(x) = s_s(x) = \bar{u}_s(x) = \bar{d}_s(x) = \bar{s}_s(x) = s(x)$, say. With this parametrization, then, the proton and neutron structure functions become

$$F_2^{ep} = \frac{x}{9}[4u_v(x) + d_v(x)] + \tfrac{4}{3}xs(x)$$

and

$$F_2^{en} = \frac{x}{9}[u_v(x) + 4d_v(x)] + \tfrac{4}{3}xs(x).$$

Consider now two extreme cases. If sea quarks are dominant we expect $F_2^{en}(x)/F_2^{ep}(x) \to 1$ and if u_v quarks are dominant the ratio should approach $\frac{1}{4}$. In figure 12.19 we show the ratio as a function of x measured in the deep inelastic region by Bodek *et al.*[14] at SLAC. At very small values of x the ratio appears to be approaching unity while at large x values it is consistent with $\frac{1}{4}$ suggesting, indeed, that sea quarks are dominant at small x and valence quarks at large x.

The quark probability functions satisfy simple *sum rules*. The proton, for example, has two u valence quarks and one d valence quark so

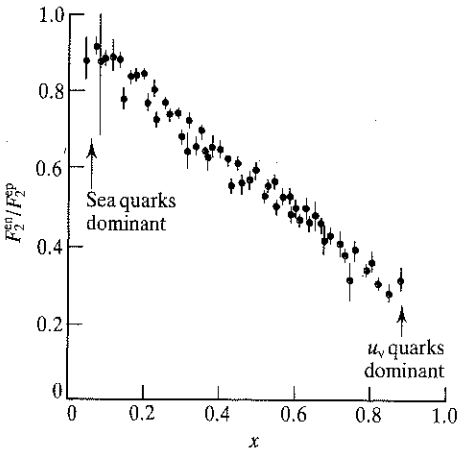

Figure 12.19
The ratio F_2^{en}/F_2^{ep} as a function of x (after Bodek K *et al.* 1974 *Phys Lett* **51B** (417).)

that

$$\int_0^1 [u(x) - \bar{u}(x)]\,dx = 2$$

$$\int_0^1 [d(x) - \bar{d}(x)]\,dx = 1.$$

Additionally, since the proton has zero strangeness,

$$\int_0^1 [s(x) - \bar{s}(x)]\,dx = 0.$$

The experimental test of these sum rules requires data on neutrino and antineutrino scattering which, as we shall see in the next section, probe the quark and antiquark distributions separately.

12.6.2 *Deep inelastic neutrino–nucleon scattering*

As a starting point for the study of ν–N scattering we take ν–e scattering as a model. The Feynman diagram for the charged-current contribution to the elastic scattering process $\nu_e + e^- \rightarrow \nu_e + e^-$ is shown in figure 12.20. In this case the reaction proceeds via the exchange of a W boson. The procedure for calculating the differential cross-section for this process is similar to that used in section 12.1 for electron–muon scattering. The currents involved here are charge-changing weak currents with the V–A structure $\gamma^\mu(1 - \gamma^5)$ rather than the pure vector electromagnetic currents γ^μ in e–μ scattering. The matrix element, provided $q^2 \ll M_W^2$ so that the propagator for the W boson approaches unity, is

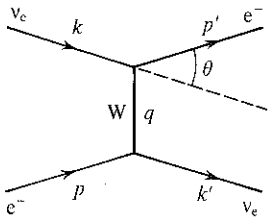

Figure 12.20
Feynman diagram for the charged-current contribution to the elastic scattering process $\nu_e + e^- \rightarrow \nu_e + e^-$.

$$\mathcal{M}_{fi} = \frac{G}{\sqrt{2}}[\bar{u}(k')\gamma^\mu(1 - \gamma^5)u(p)][\bar{u}(p')\gamma_\mu(1 - \gamma_5)u(k)]$$

where G is the Fermi coupling constant. On squaring the matrix element, summing over the final spin states and averaging over the two spin states of the initial electron (the neutrino has only one helicity state) and inserting the flux and phase space factors, we get

$$\frac{d\sigma}{d\Omega}(\nu_e e^-) = \frac{G^2 s}{4\pi^2}. \tag{12.54}$$

Here, s is the square of the total energy in the centre-of-mass system. The angular distribution (12.54) is isotropic and integration over the angles

gives for the total $\nu_e e^-$ cross-section

$$\sigma(\nu_e e^-) = \frac{G^2 s}{\pi} \approx \frac{2G^2 mE}{\pi} \tag{12.55}$$

where m is the electron mass and E is the neutrino energy in the laboratory system. The total cross-section grows linearly with the laboratory energy of the neutrino. The differential and total cross-sections for antineutrino–positron scattering are given by the same formulae. The differential cross-sections for the elastic scattering processes $\bar{\nu}_e e^- \to \bar{\nu}_e e^-$ and $\nu_e e^+ \to \nu_e e^+$, on the other hand, are given by

$$\frac{d\sigma}{d\Omega}(\bar{\nu}_e e^-) = \frac{d\sigma}{d\Omega}(\bar{\nu}_e e^+) = \frac{G^2 s}{16\pi^2}(1 - \cos\theta)^2 \tag{12.56}$$

where θ is the scattering angle in the centre-of-mass system and is defined in figure 12.21. When integrated over the angles we have

$$\sigma(\bar{\nu}_e e^-) = \sigma(\nu_e e^+) = \frac{G^2 s}{3\pi}. \tag{12.57}$$

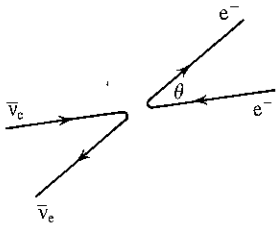

Figure 12.21
Definition of the scattering angle θ in the charged-current reaction $\bar{\nu}_e e^- \to \bar{\nu}_e e^-$.

On comparing with (12.55) we see that

$$\frac{\sigma(\bar{\nu}_e e^-)}{\sigma(\nu_e e^-)} = \frac{\sigma(\nu_e e^+)}{\sigma(\bar{\nu}_e e^+)} = \tfrac{1}{3}. \tag{12.58}$$

These differences between particle–particle and antiparticle–antiparticle scattering on the one hand, and particle–antiparticle scattering on the other, have their origin in the helicity structure of the interactions as shown in figure 12.22. For point-like (S wave) scattering, the only angular

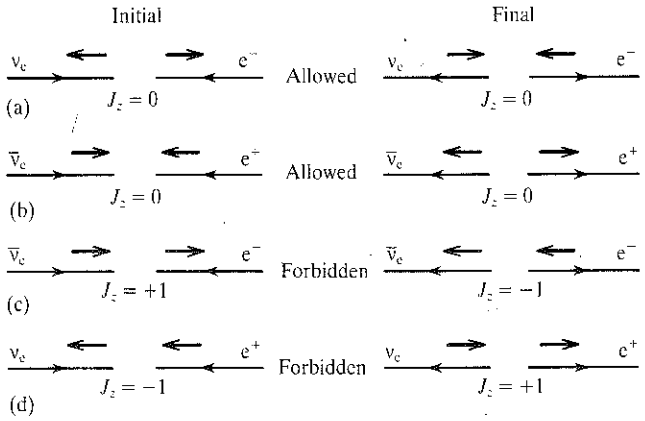

Figure 12.22
Helicity structure of the reactions (a) $\nu_e e^- \to \nu_e e^-$, (b) $\bar{\nu}_e e^+ \to \bar{\nu}_e e^+$, (c) $\bar{\nu}_e e^- \to \bar{\nu}_e e^-$ and (d) $\nu_e e^+ \to \nu_e e^+$.

momenta involved are the spins of the interacting particles. At high energies we can neglect the masses of the electron and positron; they are then left handed and right handed respectively. With the quantization axis taken as the direction of the incident $\nu_e(\bar{\nu}_e)$, backward scattering ($\theta = 0$) is forbidden by angular momentum conservation in particle–antiparticle scattering, figures 12.22(c) and 12.22(d), and hence the term $(1 - \cos\theta)^2$ in the differential cross-section. The factor $\frac{1}{3}$ in the ratios of the total cross-sections arises from the fact that the particle–antiparticle reactions have $J = 1$ and only one of the three helicity states is allowed; the cross-section is therefore reduced in comparison with the particle–particle and antiparticle–antiparticle cross-sections.

To probe the nucleon structure via the weak neutrino–nucleon interaction beams of muon-type neutrinos, for example from the decay $\pi^+ \to \mu^+\nu_\mu$, are scattered from hydrogen or heavier nuclei. We shall concentrate here on charged-current interactions, mediated by $W^\pm$ exchange, such as $\nu_\mu N \to \mu^- X$ where X is any possible hadronic final state. At the quark level, conservation of charge and lepton number constrains the possible interactions to

$$\nu_\mu d \to \mu^- u$$

$$\nu_\mu \bar{u} \to \mu^- \bar{d}$$

$$\bar{\nu}_\mu u \to \mu^+ d$$

$$\bar{\nu}_\mu \bar{d} \to \mu^+ \bar{u}.$$

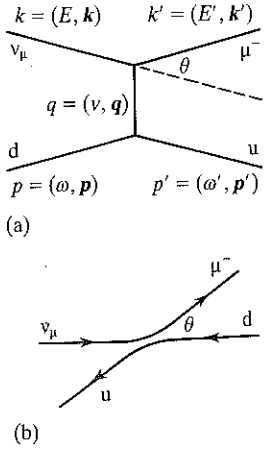

Figure 12.23
(a) Feynman diagram for the process $\nu_\mu d \to \mu^- u$; (b) the centre-of-mass scattering angle is defined as the angle between the outgoing μ^- and the incoming ν_μ.

The electromagnetic currents of the quarks are, apart from the fractional charges, the same as the lepton currents. We therefore assume that the quark weak currents are the same as the leptonic weak currents so that the cross-sections for neutrino–quark scattering can be taken over directly from the ν–e case above.

We now introduce the Lorentz scalar variable y, commonly used in the formulation of deep-inelastic scattering. In terms of the four-momenta indicated in figure 12.23(a) $y = p\cdot q/p\cdot k$. It is a simple matter to show that $y = \nu/E_{\text{lab}}$ where ν is the energy transfer and E_{lab} is the neutrino energy measured in the laboratory system. The variable y is thus the fractional energy transfer and lies in the range $0 \leqslant y \leqslant 1$. In terms of the scattering angle θ in the centre-of-mass system, defined in figure 12.23(b), $y = \frac{1}{2}(1 - \cos\theta)$ and $d\Omega = 4\pi\, dy$ (see example 12.6). Note that in this case backward scattering corresponds to $\theta = \pi$. In analogy with the ν–e differential cross-sections we have for ν–q scattering

$$\frac{d\sigma}{d\Omega}(\nu_\mu d \to \mu^- u) = \frac{d\sigma}{d\Omega}(\bar{\nu}_\mu \bar{d} \to \mu^+ \bar{u}) = \frac{G^2 \hat{s}}{4\pi^2}$$

and

$$\frac{d\sigma}{d\Omega}(\nu_\mu \bar{u} \to \mu^- \bar{d}) = \frac{d\sigma}{d\Omega}(\bar{\nu}_\mu u \to \mu^+ d) = \frac{G^2 \hat{s}}{16\pi^2}(1 + \cos\theta)^2.$$

In terms of y these become

$$\frac{d\sigma}{dy}(\nu_\mu d \to \mu^- u) = \frac{d\sigma}{dy}(\bar{\nu}_\mu \bar{d} \to \mu^+ \bar{u}) = \frac{G^2 \hat{s}}{\pi} \tag{12.59}$$

and

$$\frac{d\sigma}{dy}(\nu_\mu \bar{u} \to \mu^- \bar{d}) = \frac{d\sigma}{dy}(\bar{\nu}_\mu u \to \mu^+ d) = \frac{G^2 \hat{s}}{\pi}(1 - y)^2. \tag{12.60}$$

In these expressions, $\hat{s}$ is the square of the centre-of-mass energy in the neutrino–quark system. If x is the fraction of the four-momentum carried by quark q_i in the nucleon, $\hat{s} = xs$, where s refers to the neutrino–nucleon centre-of-mass system. As in the case of electron–nucleon scattering the differential cross-section for the inclusive process $\nu_\mu N \to \mu X$ can be regarded as an incoherent sum, over all quarks, of the differential cross-sections for the neutrino–quark processes $\nu_\mu q_i \to \mu q_f$ weighted by the quark distribution functions. Thus,

$$\frac{d^2\sigma}{dx\,dy}(\nu_\mu N \to \mu^- X) = \sum_i f_i(x_i)\left[\frac{d\sigma}{dy}(\nu_\mu q_i \to \mu q_f)\right]_{\hat{s}=xs} \tag{12.61}$$

where $f_i(x_i)$ is the quark distribution function for quark of type i.

For simplicity, consider scattering from an isoscalar target, i.e. nuclei containing equal numbers of neutrons and protons. As pointed out above, the neutrinos ν_μ interact only with d and $\bar{u}$ quarks and therefore measure the distribution functions

$$d^p(x) + d^n(x) = d(x) + u(x) \equiv Q(x) \tag{12.62}$$

$$\bar{u}^p(x) + \bar{u}^n(x) = \bar{u}(x) + \bar{d}(x) \equiv \bar{Q}(x) \tag{12.63}$$

where the notation* is that used in (12.51). On substituting the constituent cross-sections (12.59) and (12.60) and the distribution functions (12.62) and (12.63) into (12.61) we get the inclusive cross-section

$$\frac{d^2\sigma}{dx\,dy}(\nu_\mu N \to \mu^- X) = \frac{G^2 xs}{2\pi}[Q(x) + (1 - y)^2 \bar{Q}(x)]. \tag{12.64}$$

* The commonly used notation $Q(x)$ and $\bar{Q}(x)$ for the quark and antiquark distribution functions should not be confused with $Q^2 = -q^2$, the four-momentum transfer squared.

In contrast, beams of antineutrinos interact with $\bar{d}$ and u quarks and the $\bar{\nu}_\mu$N inclusive cross-section is given by

$$\frac{d^2\sigma}{dx\,dy}(\bar{\nu}_\mu N \to \mu^+ X) = \frac{G^2 xs}{2\pi}[\bar{Q}(x) + (1-y)^2 Q(x)]. \tag{12.65}$$

As in the case of e–N scattering these differential cross-sections can be written in terms of the nucleon structure functions. In terms of Q^2 and ν the result is

$$\frac{d^2\sigma^{\nu,\bar{\nu}}}{dQ^2\,d\nu} = \frac{G^2}{2\pi}\frac{E'}{E}\left[W_2^{\nu,\bar{\nu}}(Q^2,\nu)\cos^2\left(\frac{\theta}{2}\right) + 2W_1^{\nu,\bar{\nu}}(Q^2,\nu)\sin^2\left(\frac{\theta}{2}\right) \mp \frac{(E+E')}{M}W_3^{\nu,\bar{\nu}}(Q^2,\nu)\right] \tag{12.66}$$

where M is the nucleon mass. The main difference compared with the electromagnetic case is the appearance of a third structure function $W_3(Q^2, \nu)$, which arises from interference between vector and axial-vector currents; the latter are absent in the electromagnetic case. The negative sign in (12.66) applies for ν–N scattering and the positive for $\bar{\nu}$–N scattering.

In analogy with the electromagnetic case the weak interaction structure functions can be related to the cross-sections for absorption of a W boson which, because of its mass, can exist in three polarization states corresponding to right-handed, left-handed and 'scalar' bosons respectively. The relationships are of the form

$$W_1 \approx \sigma_R + \sigma_L$$
$$W_2 \approx \sigma_R + \sigma_L + 2\sigma_S$$
$$W_3 \approx \sigma_R - \sigma_L.$$

In the parity-conserving electromagnetic interaction $\sigma_R = \sigma_L$ and hence the absence of W_3 in e–N scattering. In the electromagnetic case the cross-section for transverse photons σ_T is given by $\frac{1}{2}(\sigma_R + \sigma_L)$.

The parton model predicts that the structure functions scale,

$$MW_1(Q^2,\nu) \to F_1(x) \qquad \text{and} \qquad \nu W_{2,3}(Q^2,\nu) \to F_{2,3}(x).$$

On substituting into (12.66) and changing the variables to x and y we have

$$\frac{d^2\sigma^{\nu,\bar{\nu}}}{dx\,dy} = \frac{G^2 s}{2\pi}\left[(1-y)F_2^{\nu,\bar{\nu}}(x) + y^2 xF_1^{\nu,\bar{\nu}}(x) \pm y\left(1-\frac{y}{2}\right)xF_3^{\nu,\bar{\nu}}(x)\right]. \tag{12.67}$$

In principle there are 12 weak structure functions for the nucleons, three each for ν–p, ν–n, $\bar{\nu}$–p and $\bar{\nu}$–n scattering, but if we apply charge symmetry we have

$$F_i^{\nu n} = F_i^{\bar{\nu} p} \qquad \text{and} \qquad F_i^{\bar{\nu} n} = F_i^{\nu p} \qquad (i = 1, 2, 3), \tag{12.68}$$

i.e. six independent structure functions. If we further restrict outselves to nuclei with roughly equal numbers of neutrons and protons we can form 'neutron–proton-averaged' structure functions

$$F_i^{\nu N} = \tfrac{1}{2}(F_i^{\nu n} + F_i^{\nu p}) = \tfrac{1}{2}(F_i^{\bar{\nu} p} + F_i^{\bar{\nu} n}) = F_i^{\bar{\nu} N} \equiv F_i$$

and reduce the number to three. Equation (12.67) then becomes

$$\frac{d^2\sigma^{\nu N, \bar{\nu} N}}{dx\, dy} = \frac{G^2 s}{2\pi}\left[(1-y)F_2(x) + y^2 x F_1(x) \pm y\left(1 - \frac{y}{2}\right)xF_3(x)\right]. \tag{12.69}$$

To facilitate comparison with (12.64) and (12.65) we rewrite (12.69) in powers of $1 - y$;

$$\frac{d^2\sigma^{\nu N, \bar{\nu} N}}{dx\, dy} = \frac{G^2 s}{2\pi}\left[\left(xF_1 \pm \frac{xF_3}{2}\right) + (F_2 - 2xF_1)(1-y) + \left(xF_1 \mp \frac{xF_3}{2}\right)(1-y)^2\right]. \tag{12.70}$$

We are now in a position to determine some further properties of the partons.

Fractional quark charge

From our study of e–N scattering we have seen that the partons have spin $\frac{1}{2}$ and the Callan–Gross relation, $2xF_1 = F_2$, is satisfied. The second term in (12.70) is therefore zero and

$$\frac{d^2\sigma^{\nu N, \bar{\nu} N}}{dx\, dy} = \frac{G^2 s}{4\pi}[(F_2 \pm xF_3) + (F_2 \mp xF_3)(1-y)^2]. \tag{12.71}$$

If we compare, for example, this expression for ν–N scattering with (12.64), we find

$$F_2^{\nu N}(x) = 2x[Q(x) + \bar{Q}(x)] \tag{12.72a}$$

$$xF_3^{\nu N}(x) = 2x[Q(x) - \bar{Q}(x)]. \tag{12.72b}$$

By comparing $F_2^{\nu N}$ with F_2^{eN} it is possible to check the fractional charge

values assigned to the quarks. On combining (12.52) and (12.53) we find, for an isoscalar target,

$$F_2^{eN} = x\{\tfrac{5}{18}[u(x) + \bar{u}(x) + d(x) + \bar{d}(x)] + \tfrac{1}{9}[s(x) + \bar{s}(x)]\}. \tag{12.73}$$

From (12.62), (12.63) and (12.72a) we obtain

$$F_2^{\nu N} = x[d(x) + u(x) + \bar{u}(x) + \bar{d}(x)]. \tag{12.74}$$

Thus,

$$\frac{F_2^{eN}}{F_2^{\nu N}} \geqslant \tfrac{5}{18}$$

where the equality holds if we neglect the s and $\bar{s}$ quark contributions. The numerical value of the ratio is just the mean square charge of the u and d quarks.

The fractional charge hypothesis is well supported by experiment. In figure 12.24 we show a comparison of $F_2^{\nu N}$ measured in the heavy-liquid bubble chamber Gargamelle at CERN and F_2^{eN} measured at SLAC in the same q^2 region.

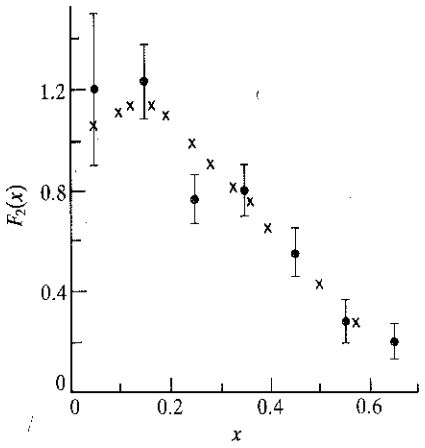

Figure 12.24 Comparison of $F_2^{\nu N}$ (•), measured in the heavy-liquid bubble chamber Gargamelle at CERN, and F_2^{eN} (×), measured at SLAC, in the region $Q^2 > 1$. The electron results have been multiplied by 18/5; see text for details. (From Perkins D H 1986 *Introduction to High Energy Physics* Addison-Wesley.)

Number of valence quarks

From (12.72b) it can be seen that $F_3^{\nu N}$ measures the difference between quark and antiquark concentrations in the nucleon. Since the sea contains equal numbers of quarks and antiquarks the integral of $F_3^{\nu N}(x)$ must equal

the number of valence quarks, i.e.

$$\int_0^1 F_3^{\nu N}(x)\,dx = 3.$$

This sum rule, known as the Gross–Llewellyn Smith sum rule has been verified by de Groot *et al.*[15] and Benvenuti *et al.*[16] who obtained values of 3.2 ± 0.5 and 2.8 ± 0.6 respectively.

Quark and antiquark distribution functions

Measurements of the differential cross-sections for ν–N and $\bar{\nu}$–N deep-inelastic scattering permit the quark and antiquark distribution functions to be separated. Specifically, if we add and substruct $d^2\sigma^{\nu N}/dx\,dy$ and $d^2\sigma^{\bar{\nu}N}/dx\,dy$, and assume that the Callan–Gross relation holds, then

$$\frac{d^2\sigma^{\nu N}}{dx\,dy} + \frac{d^2\sigma^{\bar{\nu}N}}{dx\,dy} = \frac{G^2 s}{2\pi}\{F_2[1 + (1-y)^2]\} \tag{12.75}$$

$$\frac{d^2\sigma^{\nu N}}{dx\,dy} - \frac{d^2\sigma^{\bar{\nu}N}}{dx\,dy} = \frac{G^2 s}{2\pi}\{xF_3[1 - (1-y)^2]\}. \tag{12.76}$$

From these relations $F_2(x)$ and $F_3(x)$ can be determined and hence, through (12.72), the quark and antiquark distribution functions may be obtained. Figure 12.25 shows typical quark and antiquark momentum distributions in the nucleon obtained from measurements at CERN and Fermilab. The antiquarks, which must come from the quark–antiquark sea, are concentrated at low values of x and at very low values of x the sea is dominant. The valence quark distribution, shown by the dashed line, peaks around $x \approx 0.2$ and is dominant at higher values of x. These findings are in accord with those from e–N scattering.

The need for gluons

If the nucleon is made entirely from quarks and antiquarks then the integrals of the structure functions, or equivalently the sum of the fractional momenta of all the constituents, should be unity; the total momentum of the constituents should equal the momentum of the nucleon. Thus we expect

$$\frac{18}{5}\int_0^1 F_2^{eN}(x)\,dx = \int_0^1 F_2^{\nu N}(x)\,dx$$
$$= \int_0^1 x[u(x) + \bar{u}(x) + d(x) + \bar{d}(x)]\,dx \approx 1.$$

The data shown in figure 12.25 give a value of about 0.5 for these integrals

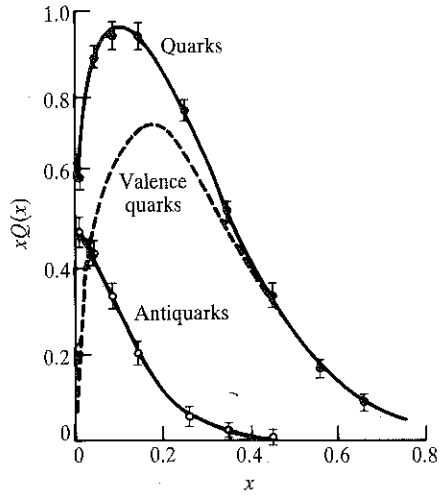

Figure 12.25 Momentum distributions of quarks and antiquarks in the nucleon. As explained in the text, the sum of the differential cross-sections for νN and $\bar{\nu}$N measures the structure function F_2 and the difference F_3. From these the quark and antiquark distribution functions can be obtained through equations (12.72). The difference between the quark and antiquark distributions gives the valence quark distribution shown by the broken line. This peaks around $x \approx 0.2$ and is dominant at large x. The antiquarks from the sea are concentrated towards small x and for very small values of x the sea is dominant. (From Perkins D H 1986 *Introduction to High Energy Physics* Addison-Wesley.)

implying that the quarks carry only about one-half of the momentum of the proton. The momentum fraction carried by the strange quarks in the nucleon can be safely ignored in these considerations. We are therefore forced to the conclusion that roughly half the momentum of the proton must be carried by constituents other than the quarks which are 'invisible' to both the electromagnetic and weak probes. These constituents, which possess neither electric nor weak charge, are called gluons; they carry colour or strong charge and are responsible for binding the quarks together inside the nucleon.

12.6.3 Summary

Deep inelastic scattering experiments have produced firm dynamical evidence for the existence of quarks and gluons. Whether probed by virtual photons or W bosons the same internal structure of the nucleon is revealed. The phenomenon of scaling indicates that the constituents are point-like or structureless; at high values of Q^2 and ν the structure functions are functions only of the single variable $x = Q^2/2M\nu$. $F(Q^2, \nu) \rightarrow F(x)$ as Q^2 and ν approach infinity while x remains finite. The variable x turns out to be the fraction of the momentum carried by the partons. The Callan–Gross relation, $2xF_1 = F_2$, is well supported by experiment

indicating that the partons have spin $\frac{1}{2}$. The ratio of the structure functions from e–N scattering, F_2^{eN}, and ν–N scattering, $F_2^{\nu N}$, supports the hypothesis that the (charged) partons have fractional charges which we identify as the quarks. Only about 50 per cent of the momentum of the nucleon is carried by the quarks, the remainder being carried by gluons. The quark–antiquark sea is confined to low values of x while the valence quarks are dominant at high x values.

The nucleon then is a fairly complex particle. The proton, for example, may be visualized as containing three valence quarks u_v, u_v and d_v which carry a large fraction of the momentum of the proton. As they move in their mutual field they may emit gluons in a bremsstrahlung-like process. These in turn give rise to a predominantly low-momentum sea of quark–antiquark pairs.

12.7 *The Drell–Yan process*

The Drell–Yan process is the name associated with the inclusive production of di-leptons in hadron–hadron collisions, $h + h \rightarrow l^+ + l^- + X$. It is important in several respects. First, it provides a further test of the parton model and, secondly, it allows the structure functions of hadrons other than nucleons to be determined. In addition, it provides a mechanism for the production of $W^{\pm}$ and Z^0 bosons in hadron–hadron collisions. Our main concern here is with the parton model predictions and the structure functions of hadrons.

The process can be visualized as in figure 12.26. We restrict ourselves to centre-of-mass energies which are sufficiently large that masses and transverse momenta of the quarks and leptons are negligible. The incoming hadrons h_1 and h_2, with four-momenta p_1 and p_2, consist of quarks and antiquarks with distribution functions $q_i(x)$ and $\bar{q}_i(x)$ respectively; the index i represents the different quark flavours. The constituent process, responsible for the production of lepton pairs l^+l^- with mass M, is shown as $q_i\bar{q}_i \rightarrow \gamma^* \rightarrow l^+l^-$. A quark and an antiquark of the same flavour fuse to produce a virtual photon γ^* which then materializes into

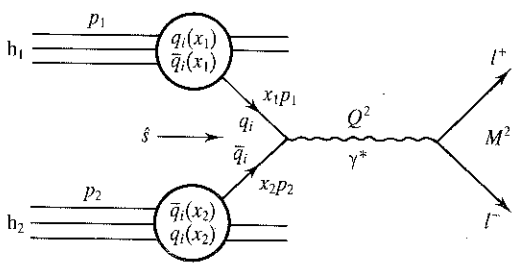

Figure 12.26
The Drell–Yan process in the parton model.

the lepton pair. If quark q_i has a momentum fraction x_1 and antiquark $\bar{q}_i$ a momentum fraction x_2, the centre-of-mass energy $\hat{s}$ for the constituent process is

$$\hat{s} = (x_1 p_1 + x_2 p_2)^2 \approx x_1 x_2 s = Q^2 = M^2. \tag{12.77}$$

The cross-section for this point-like constituent process is

$$\hat{\sigma}(q_i \bar{q}_i \to l^+ l^-) = \frac{4\pi\alpha^2}{3\hat{s}} e_{q_i}^2 \tag{12.78}$$

where e_{q_i} is the charge of quark q_i in units of e. To obtain the cross-section for the process $h_1 h_2 \to l^+ l^- X$ we follow the procedure used in deep-inelastic scattering, i.e. we form the incoherent sum of the constituent cross-sections for all quarks. Thus,

$$d^2\sigma(h_1 h_2 \to l^+ l^- X) = \tfrac{1}{3} \frac{4\pi\alpha^2}{3M^2} \sum_i e_{q_i}^2 [q_i(x_1)\bar{q}_i(x_2) + \bar{q}_i(x_1) q_i(x_2)] dx_1\, dx_2. \tag{12.79}$$

Here, $q_i(x_1)$ is the probability that a quark of flavour i carries the momentum fraction x_1 in hadron h_1 and $\bar{q}_i(x_2)$ the probability that an antiquark of the same flavour carries momentum fraction x_2 in hadron h_2. The second term in the square brackets allows for the probability that the antiquark comes from h_1 and the quark from h_2. The extra factor $\frac{1}{3}$ is a colour factor. This takes account of the fact that the virtual photon is a colour singlet so that there must be appropriate matching of the colours of the annihilating quarks; for three colours the probability that a red quark annihilates with an antired antiquark, for example, is $\frac{1}{3}$.

In order to compare the basic equation for the differential cross-section (12.79) with experiment, we recast it in terms of measurable variables. For example, the differential cross-section for the production of a lepton pair of mass M may be written

$$\frac{d\sigma}{dM^2} = \int dx_1\, dx_2 \frac{d^2\sigma}{dx_1\, dx_2} \delta(M^2 - x_1 x_2 s). \tag{12.80}$$

The δ function ensures that the kinematic constraint $M^2 = x_1 x_2 s$ is satisfied. On substitution of $d^2\sigma/dx_1 dx_2$ from (12.79) we obtain

$$\frac{d\sigma}{dM^2} = \frac{4\pi\alpha^2}{9M^4} \int dx_1\, dx_2\, x_1 x_2\, \delta(x_1 x_2 - \tau) \times \sum_i e_{q_i}^2 [q_i(x_1)\bar{q}_i(x_2) + \bar{q}_i(x_1) q_i(x_2)] \tag{12.81}$$

where the dimensionless variable $\tau = M^2/s$. Upon integration we obtain a function $F(\tau)$ so that, although the cross-section depends on M^2 and s, it does so only through the ratio $\tau = M^2/s$, i.e. the quantity

$$M^4 \frac{d\sigma}{dM^2} = \tfrac{4}{9}\pi\alpha^2 F\left(\frac{M^2}{s}\right) \tag{12.82}$$

should exhibit scaling.

A frequently used variable in the study of the Drell–Yan process is the Feynman scaling variable $x_F = x_1 - x_2$. A measurement of the four-momenta of the leptons determines M^2 and x_F and hence fixes the x values of the annihilating quark and antiquark. In terms of M and x_F the differential cross-section is

$$\frac{d^2\sigma}{dM\, dx_F} = \frac{8\pi\alpha^2}{9M^3} \frac{\tau}{(x_F^2 + 4\tau)^{1/2}} \sum_i e_{q_i}^2 [q_i(x_1)\bar{q}_i(x_2) + \bar{q}_i(x_1) q_i(x_2)]. \tag{12.83}$$

The scaling behaviour of this cross-section and hence the validity of the parton model is displayed in figure 12.27 which shows data on inclusive di-muon production in pp collisions at values of $\sqrt{s}$ in the range 24–62 GeV.

In proton–proton collisions the quark and antiquark distribution functions appearing in (12.83) are just those determined from deep inelastic lepton–proton scattering which may therefore be used to predict

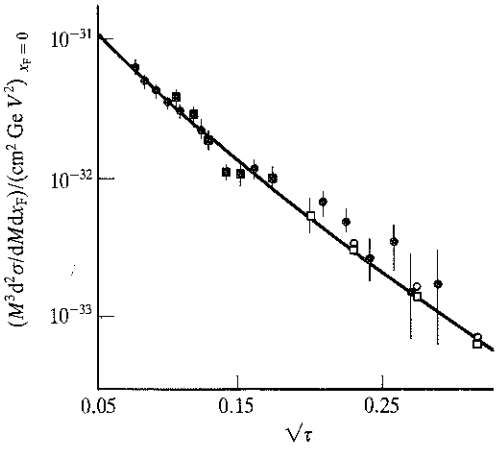

Figure 12.27 Experimental test of scaling in di-muon production in pp collisions. The differential cross-section $M^3(d^2\sigma/dM\, dx_F)$ at $x_F = 0$, measured over a range of $\sqrt{s}$ from 24 to 62 GeV, depends only on the scaling variable $\tau = M^2/s$ where M is the di-muon mass: ○, 23.8 GeV; □, 27.4 GeV; ■, 44 GeV; ●, 62 GeV. (After Kenyon I R 1982 *Rep Prog Phys* **45** (1213).)

Table 12.1
The x dependence of the valence and sea quark distributions, $xq(x)$, in the nucleon and the pion

	Nucleon	Pion
Valence quarks	$x^{1/2}(1-x)^3$	$x^{1/2}(1-x)$
Sea quarks	$(1-x)^7$	$(1-x)^5$

the cross-section for $pp \to \mu^+\mu^- X$. On the other hand the Drell–Yan process enables the pion structure functions to be determined by measuring the cross-sections for the processes $\pi^\pm p \to \mu^+\mu^- X$. It is found that the valence quarks in the mesons are 'harder' than those in the nucleon; the valence quarks in a meson carry about one and a half times the momentum fraction carried by the valence quarks in a nucleon. This is consistent with the view that a meson consists of a $q\bar{q}$ pair of valence quarks while the nucleon has three valence quarks. Table 12.1 compares the quark distribution functions $xq(x)$ of the valence and sea quarks in nucleons and pions.

12.8 *Quark jets in e^+e^- annihilation*

The production of hadrons in electron–positron annihilation at high energies is closely related to the Drell–Yan process. Consider first the reaction $e^+e^- \to \mu^+\mu^-$, which is described in lowest order by the Feynman diagram in figure 12.28(a). The differential cross-section for this process is

$$\frac{d\sigma}{d(\cos\theta)} = \frac{\pi\alpha^2}{2s}(1+\cos^2\theta) \tag{12.84}$$

where $\sqrt{s}$ is the energy in the centre-of-mass system and θ is the angle between the μ^- and the incident e^-. On integrating (12.84) we get for the total cross-section

$$\sigma(e^+e^- \to \mu^+\mu^-) = \frac{4\pi\alpha^2}{3s}. \tag{12.85}$$

A possible mechanism for hadron production in the process $e^+e^- \to$ hadrons is simply obtained from figure 12.28(a) by replacing the muons by quarks as in figure 12.28(b). The electron and positron annihilate to produce a virtual photon which then materializes into a $q\bar{q}$ pair. The cross-section for this process is

$$\sigma(e^+e^- \to q_i\bar{q}_i) = \frac{4\pi\alpha^2}{3s}e_{q_i}^2 \tag{12.86}$$

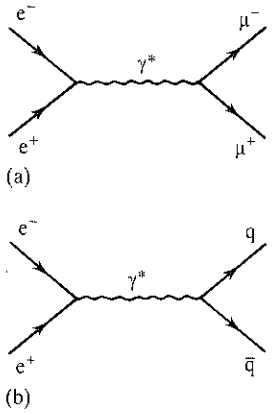

Figure 12.28
Lowest order Feynman diagrams for the processes (a) $e^+e^- \to \mu^+\mu^-$ and (b) $e^+e^- \to q\bar{q}$.

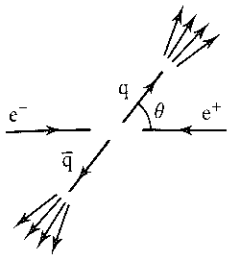

Figure 12.29
Schematic diagram of the production of two 'back-to-back' hadron jets in e^+e^- annihilation.

where e_{q_i} is the charge of the quark with flavour i in units of the charge on the electron. Of course, the quarks do not appear as free particles in the laboratory – they must 'fragment' into colourless hadrons. In this fragmentation process the momenta of the hadrons transverse to the line of flight of the parent quark are restricted to values of the order of a few hundred MeV/c so that at high centre-of-mass energies the hadrons appear 'back to back' in narrow cones or jets as in figure 12.29. A typical two-jet event is shown in figure 12.30. The axis of a jet may be determined, for instance, by finding the angle θ, with respect to the incident beam direction, along which the sum of the longitudinal momenta of the hadrons in the jet is maximized. The evidence that the hadrons really originate from a spin $\frac{1}{2}$ quark is that the angular distribution of the jet axes is given by (12.84); spin 0 partons would give rise to a $\sin^2\theta$ distribution in disagreement with experimental results.

Although the hadrons retain a 'memory' of the quark from which they originate, we assume that the fragmentation process does not affect the cross-section for the process $e^+e^- \to q\bar{q} \to$ hadrons and we are led to the simple and remarkable prediction that at high energies

$$R = \frac{\sigma(e^+e^- \to \text{hadrons})}{\sigma(e^+e^- \to \mu^+\mu^-)} = 3\sum_i e_{q_i}^2. \tag{12.87}$$

The factor 3 arises because of the three possible colour combinations of the $q\bar{q}$ pair.

The ratio R is shown as a function of centre-of-mass energy in

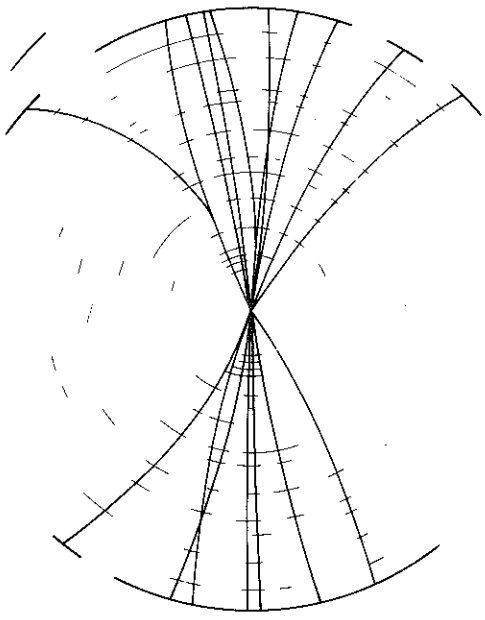

Figure 12.30
Sketch of a typical two-jet event viewed along the beam line in e^+e^- annihilation.

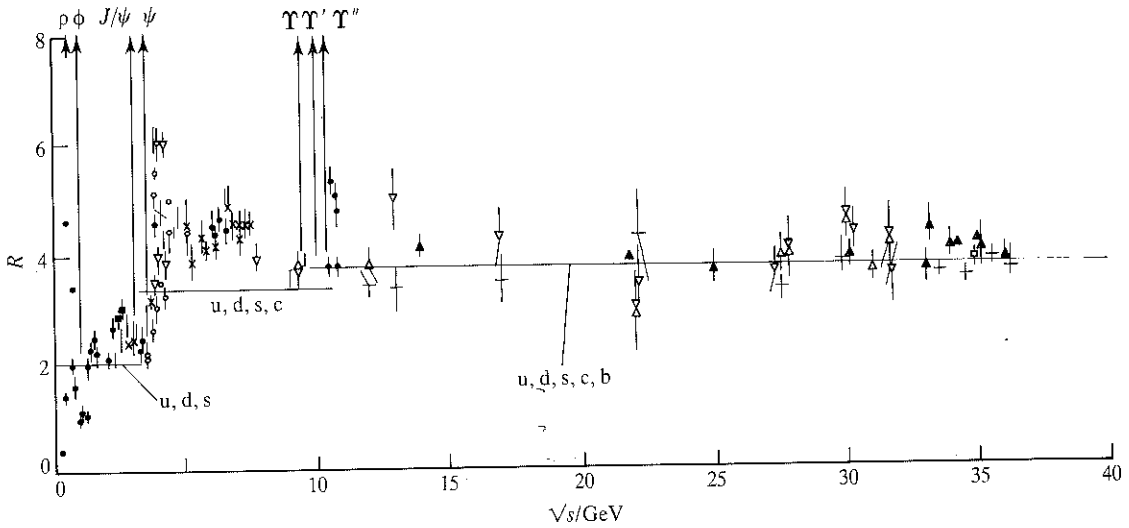

Figure 12.31 Plot of the ratio R, defined in equation (12.88) as a function of the total centre-of-mass energy. The sharp peaks correspond to the production of narrow vector meson resonances.

figure 12.31. For the light quarks u, d and s with charges $+\frac{2}{3}$, $-\frac{1}{3}$ and $-\frac{1}{3}$ respectively, R is predicted to be 2. The charmed quark threshold is around $s = 9\ \text{GeV}^2$ and below this value there is reasonable agreement between the experimental results and the prediction. Above the upsilon states ($b\bar{b}$), i.e. above the b quark threshold, R is expected to be

$$R = 3[(\tfrac{2}{3})^2 + (-\tfrac{1}{3})^2 + (-\tfrac{1}{3})^2 + (\tfrac{2}{3})^2 + (-\tfrac{1}{3})^2] = 3\tfrac{2}{3} \qquad (12.88)$$

in good agreement with the data. This may be regarded as further confirmation of the validity of the quark parton model and equally importantly firm evidence for the existence of colour.

REFERENCES 12

1 **Mott N F** 1929 *Proc Roy Soc* **A124** (425)

2 **Rosenbluth M N** 1950 *Phys Rev* **79** (615)

3 **Hofstadter R and McAllister R W** 1955 *Phys Rev* **98** (217)

4 **Halzen F and Martin A D** 1984 *Quarks and Leptons: An Introductory Course in Modern Particle Physics* Wiley pp. 88–91

5 **Gasiorowicz S** 1966 *Elementary Particle Physics* Wiley p. 435

6 **Hughes E B** *et al.* 1965 *Phys Rev* **139B** (458)

7 **Hofstadter R** 1956 'Electron scattering and nuclear structure' *Rev Mod Phys* **28** (214)

8 **Bartel W** *et al.* 1968 *Phys Lett* **28B** (148)

9 **Miller G** *et al.* 1972 *Phys Rev* **D5** (528)

10 **Friedman J I and Kendall H W** 1972 *Ann Rev Nucl Sci* **22** (203)

11 **Feynman R P** 1969 *Phys Rev Lett* **23** (1415)

12 **Callan C G and Gross D** 1969 *Phys Rev Lett* **22** (156)

13 **Aitchison I J R and Hey A J G** 1982 *Gauge Theories in Particle Physics* Adam Hilger pp. 96–9

14 **Bodek K** *et al.* 1974 *Phys Rev* **51B** (417)

15 **de Groot J G H** *et al.* 1979 *Z Phys* **C1** (143)

16 **Benvenuti A** *et al.* 1979 *Phys Rev Lett* **42** (1317)

EXAMPLES 12

12.1 Show that equation (12.18) follows from equation (12.17) if terms of order m^2, where m is the electron mass, are neglected.

12.2 With reference to figure 12.5 evaluate equation (12.18) in the laboratory frame to show that, neglecting the electron mass,

$$\overline{|\mathscr{M}|^2} = \frac{8e^4}{q^2} 2EE'M^2\left[\cos^2\left(\frac{\theta}{2}\right) - \frac{q^2}{2M^2}\sin^2\left(\frac{\theta}{2}\right)\right].$$

12.3 If the charge density distribution of the proton, $\rho(\boldsymbol{r}) = \rho_0 \exp(-m\boldsymbol{r})$, is normalized to unity show, using equation (12.4), that the form factor is given by

$$F(q) = \frac{m^4}{(m^2 + q^2)^2}.$$

If $m^2 = 0.71\ \text{GeV}^2$ determine the root-mean-square radius of the charge distribution.

12.4 For small values of $|\boldsymbol{q}|$ the proton form factor may be expressed as

$$F(q) = \int\left[1 + \mathrm{i}\boldsymbol{q}\cdot\boldsymbol{r} - \frac{(\boldsymbol{q}\cdot\boldsymbol{r})^2}{2!} + \cdots\right]\rho(\boldsymbol{r})\,\mathrm{d}\tau.$$

Assuming $\rho(\boldsymbol{r})$ is spherically symmetric and normalized so that $\int \rho(\boldsymbol{r})\,\mathrm{d}\tau = 1$, show that the mean square radius of the charge distribution is

$$\langle r^2\rangle = -6\frac{\partial F(q)}{\partial q^2}.$$

Hence calculate the root-mean-square radius for the proton using the result of example 12.3 and evaluating the derivative at $q^2 = 0$. Take $m^2 = 0.71\ \text{GeV}^2$.

12.5 The frame of reference used in the parton model is one in which the proton has such a large momentum that all masses may be neglected – the so-called infinite momentum frame. In this frame suppose the proton has four-momentum $p = (E, P) = (p, 0, 0, P)$. The proton is visualized as a stream of partons each with zero momentum *transverse* to the direction of motion of the proton and each carrying some variable fraction x of the four-momentum, energy and mass of the proton. With reference to figure 12.16 show that x is precisely the Bjorken scaling variable

$$x = -\frac{q^2}{2Mv} = \frac{Q^2}{2Mv}$$

where M is the proton mass. Hence show that $v = Q^2/2m$ where m is the struck parton mass.

12.6 The Lorentz scalar y was defined in the text as $y = (p \cdot q)/(p \cdot k)$ (see figure 12.23). Show that

$$y = v/E_{\text{lab}} = \tfrac{1}{2}(1 - \cos\theta)$$

where v is the energy transfer, E_{lab} is the neutrino energy in the laboratory system and θ is the scattering angle in the centre-of-mass system. Hence, show that the element of solid angle is $\mathrm{d}\Omega = 4\pi\,\mathrm{d}y$.